# Artificial Photosynthetic Reaction Centers with Porphyrins as Primary Electron Acceptors†

**Stephanie L. Gould, Gerdenis Kodis, Rodrigo E. Palacios, Linda de la Garza, Alicia Brune, Devens Gust,* Thomas A. Moore,* and Ana L. Moore***

*The Center for the Study of Early Events in Photosynthesis, Department of Chemistry and Biochemistry, Arizona State University, Tempe, Arizona 85287-1604*

*Received: February 17, 2004; In Final Form: April 6, 2004*

A triad consisting of a carotenoid (C), a dimesitylporphyrin (P), and a tris(heptafluoropropyl)porphyrin ($P_F$), C−P−$P_F$, has been synthesized and found to undergo rapid singlet−singlet energy transfer between the porphyrin moieties so that their excited states are in equilibrium. Photoinduced electron transfer from the first excited singlet state of P, or hole transfer from the first excited singlet state of $P_F$, yields C−$P^{\bullet+}$−$P_F^{\bullet-}$. Electron transfer from C then yields the final charge-separated state $C^{\bullet+}$−P−$P_F^{\bullet-}$ with a quantum yield of 0.73 and a lifetime of 500 ns in tetrahydrofuran solution at ambient temperature. The final charge-separated state decays to form primarily a triplet excited state localized on the carotenoid, $^3$C−P−$P_F$, rather than the ground state. A second triad in which P is metalated ($P_{Zn}$) has also been synthesized. In this system, the excited singlet states of the porphyrins are no longer in equilibrium; fast electron transfer from excited $P_{Zn}$ to $P_F$ to form C−$P_{Zn}^{\bullet+}$−$P_F^{\bullet-}$ and also fast energy transfer from $P_{Zn}$ to $P_F$ with subsequent hole transfer from $P_F$ to $P_{Zn}$ converge to give the same C−$P_{Zn}^{\bullet+}$−$P_F^{\bullet-}$ species, which evolves to $C^{\bullet+}$−$P_{Zn}$−$P_F^{\bullet-}$ with a quantum yield of 0.14. This state decays to $^3$C−$P_{Zn}$−$P_F$ with a quantum yield of 0.06 in tetrahydrofuran at room temperature. The charge recombination reaction follows a single-step mechanism for $C^{\bullet+}$−P−$P_F^{\bullet-}$ from room temperature to 77 K and for $C^{\bullet+}$−$P_{Zn}$−$P_F^{\bullet-}$ below 250 K. Above 250 K, a two-step pathway is accessed for the recombination reaction of $C^{\bullet+}$−$P_{Zn}$−$P_F^{\bullet-}$ in addition to the direct recombination mechanism. This new pathway involves an endergonic step to populate C−$P_{Zn}^{\bullet+}$−$P_F^{\bullet-}$ having an $E_a$ of ∼0.23 eV. Certain photophysical characteristics of these triads, in particular the recombination to the triplet state, are reminiscent of those of artificial reaction centers with $C_{60}$ as the primary electron acceptor.

## Introduction

Ensembles of covalently linked donors and acceptors have been used successfully to model the stepwise electron transfer process observed in the reaction centers of photosynthetic organisms. In early reaction center models, quinones were used extensively as primary electron acceptors.[1−3] More recently fullerene derivatives emerged as appealing alternatives to quinones as electron acceptors.[4−7] One of the attractive features of $C_{60}$ derivatives in photoinduced electron-transfer reactions is their small total reorganization energy ($\lambda$).[6,8−12] According to the Marcus−Hush treatment, $\lambda$ is one of the key parameters controlling the dynamics of electron-transfer processes.[13−16] Low reorganization energy results in faster forward rates at lower driving force, which a priori shift charge recombination further into the "inverted region" and thereby slow this energy-wasting step.

In addition, the energy of the fullerene radical anion is less affected by solvent dielectric properties and mobility than are those of the anions of moieties such as quinones. Thus, the thermodynamic driving force for electron-transfer reactions involving fullerenes ($-\Delta G°$, another key parameter affecting the rate of electron transfer) does not change as drastically as the solvent is made less polar or frozen into a glassy state.[11,17] This allows photoinduced electron transfer in some porphyrin−fullerene systems to occur at temperatures as low as 8 K.[6,18] The early steps of photosynthetic electron transfer can also occur at very low temperatures.

In our mimicry of photosynthesis, we have used energetic charge-separated states generated with artificial reaction centers inserted vectorially into model lipid bilayers to drive the transport of ions across such membranes.[19−21] For our initial investigations we employed artificial reaction centers (triads) with quinones as the primary electron acceptors. Because of their involved synthesis, inherent instability, and poor yield of the final charge separation in low dielectric media, we designed alternative reaction center mimics to use in model membranes. As mentioned above, $C_{60}$-based constructs are in principle appealing options. However, to date we and others[22,23] have found that the lipid aggregation/insolubility of $C_{60}$ derivatives limits their use in membranes.

Porphyrins are desirable alternatives to quinones and even $C_{60}$ as electron acceptors. Indeed, cyclic tetrapyrroles are the initial electron acceptors in all types of reaction centers in natural photosynthesis. Previously, we have reported the dependence of electron-transfer rates in porphyrin dyads on structure, thermodynamic driving force, and solvent.[24,25] Although there are structural reasons to expect that the reorganization energies of porphyrins could be larger than that of $C_{60}$, they are also expected to be considerably lower than those of quinones. Here, we report the synthesis and spectroscopic study of triads **1** and **1′** in which porphyrins are the primary electron donors and acceptors; **1** and **1′** are models for amphipathic triads suitable

† Part of the special issue "Gerald Small Festschrift".

* Corresponding authors. E-mail: gust@asu.edu (D.G.), tmoore@asu.edu (T.A.M.), amoore@asu.edu (A.L.M).

10.1021/jp040143y CCC: $27.50 
Published on Web 06/08/2004

for insertion into membranes. Triad **1** consists of a carotenoid moiety (C) linked to a dimesityl free base porphyrin (P), which is connected in series to a fluorinated free base porphyrin ($P_F$); a carboxylic acid attached to $P_F$ would render the triad amphipathic. In **1′**, P is replaced by a dimesityl zinc porphyrin ($P_{Zn}$). As described below, excitation of the free base porphyrin and/or the fluorinated porphyrin in C−P−$P_F$ in tetrahydrofuran solution is followed by fast singlet−singlet energy exchange between the porphyrins and slower electron and/or hole transfer, forming the initial charge-separated state $C-P^{\bullet+}-P_F^{\bullet-}$. This charge-separated state evolves into a long-lived charge-separated state, $C^{\bullet+}-P-P_F^{\bullet-}$, which finally decays, forming mostly a triplet excited-state localized on the carotenoid, $^3C-P-P_F$, rather than the ground state. Triad **1′** shows fast direct electron transfer from $^1P_{Zn}$ to $P_F$ to form $C-P_{Zn}^{\bullet+}-P_F^{\bullet-}$ and also fast energy transfer from $^1P_{Zn}$ to $P_F$ with subsequent hole transfer from $^1P_F$ to $P_{Zn}$ to converge to the same $C-P_{Zn}^{\bullet+}-P_F^{\bullet-}$, which finally evolves to $C^{\bullet+}-P_{Zn}-P_F^{\bullet-}$. As discussed below, these photochemical characteristics, in particular the recombination to the triplet state, match quite closely those of triads with $C_{60}$ as the primary electron acceptor.[6,11,17,18,26]

## Results

**Synthesis.** The required dimesityl porphyrin, 5,15-bis(4-carbomethoxyphenyl)-10,20-bis(2,4,6-trimethylphenyl)porphyrin (**7**), and apocarotenoid were prepared by published procedures.[27,28] Hydrolysis of one of the ester groups of **7** under acid conditions, followed by a Curtius rearrangement and deprotection of the remaining ester group, afforded the amino acid porphyrin (**11**), which is the central building block of triad **1**. The dipyrromethane required for the synthesis of the fluorinated porphyrin was obtained by reaction of pyrrole and heptafluorobutaraldehyde in tetrahydrofuran with catalytic amounts of hydrochloric acid. Condensation of this dipyrromethane with heptafluorobutaraldehyde and 4-formylmethylbenzoate[29] resulted in three porphyrins, including 5-(4-carbomethyoxyphenyl)-10,15,20-tris(heptafluoropropyl)porphyrin, **4**. Because of the sensitivity of the fluorinated porphyrin to bases, the hydrolysis of the methyl ester of **4** had to be carried out under acidic conditions, with trifluoroacetic acid/hydrochloric acid. Dyad **2** was obtained by coupling the acid chloride of the fluorinated porphyrin with the required dimesityl porphyrin. Similar coupling techniques were employed in the syntheses of triad **1** and model dyad **5**. Zinc compounds **1′** and **2′** were synthesized by adding an excess of zinc acetate in a methanol/dichloromethane solution to a dichloromethane solution of the triad/dyad with careful monitoring; when the dimetalated product started to form, the reaction mixture was immediately chromatographed. Compounds **3′** and **5′** were prepared simply by treating the porphyrin or the carotenoporphyrin with an excess of zinc acetate and allowing the reaction to proceed until the metalation of the porphyrin was completed.

**Cyclic Voltammetry.** To estimate the energies of the charge-separated states, electrochemical measurements were undertaken to investigate the redox properties of triad **1** and model compounds **3**, **3′**, and **4**. The measurements were performed in benzonitrile containing 0.1 M tetra-*n*-butylammonium hexafluorophosphate and ferrocene as an internal standard (oxidation at 0.458 V vs SCE). The data below are reported vs SCE. The oxidation and reduction processes of porphyrins were quasi-reversible, whereas the carotenoid oxidation was irreversible and the peak potential is given in this case. Free base dimesitylporphyrin **3** featured oxidation waves at 1.03 and 1.32 V and reduction at −1.19 V. Free base fluorinated porphyrin **4** showed an oxidation at 1.59 V and a reduction at −0.63 V. Model porphyrin **3′** exhibited an oxidation at 0.76 V and a reduction at −1.34 V.

Triad **1** was found to exhibit a first oxidation potential of 0.52 V, which corresponds to the carotenoid oxidation,[30] a second oxidation potential of 1.06 V, which corresponds to oxidation of the free base dimesitylporphyrin moiety, a first reduction potential of −0.62 V, which corresponds to the fluorinated free base porphyrin, and a second reduction potential of −1.18 V, which corresponds to the first reduction of the dimesityl free base porphyrin. The potentials measured for the triad are very similar to those measured for model porphyrins, indicating that linking the moieties in the triad does little to perturb the individual redox centers.

The energies of the $C-P^{\bullet+}-P_F^{\bullet-}$, $C^{\bullet+}-P^{\bullet-}-P_F$, $C^{\bullet+}-P-P_F^{\bullet-}$, $C-P_{Zn}^{\bullet+}-P_F^{\bullet-}$, $C^{\bullet+}-P_{Zn}^{\bullet-}-P_F$, and $C^{\bullet+}-P_{Zn}-P_F^{\bullet-}$ charge-separated states were estimated as 1.68, 1.70, 1.14, 1.38, 1.86, and 1.14 eV, respectively, based on the electrochemically determined oxidation and reduction potentials of porphyrins and carotenoid in triad **1** and model porphyrin **3′**.

**Absorption Spectra.** The absorption spectrum of **1** in tetrahydrofuran is shown in Figure 1a. Absorption maxima are at 647, 593, 548, 509, 476, 421, 405(sh), 375(sh), and 300 nm. For comparison, the spectra of model compounds **2**, **3**, and **4** are also shown. Absorption maxima for the dimesityl free base porphyrin **3** and fluorinated free base porphyrin **4** are at 650, 594, 550, 515, 419, 402(sh), 300 nm, and 644, 591, 546, 511, 410, and 375(sh) nm, respectively. The absorption spectrum of model dyad **2** is essentially a linear combination of the absorption spectra for **3** and **4**, with maxima at 647, 593, 549, 514, 420, 405(sh), 375(sh), and 300 nm. The difference between the absorption spectra of **1** and **2** corresponds to the absorption due to the carotenoid in the triad.

The absorption spectrum of **1′** in tetrahydrofuran is shown in Figure 1b. Absorption maxima are at 645, 598, 559, 509, 476, 428, 405(sh), 375(sh), and 310 nm. For comparison, the spectra of model compounds **2′**, **3′**, and **4** are also shown. Absorption maxima for the dimesityl zinc porphyrin **3′** are at 600, 560, 522, 428, 408(sh), and 312 nm. A linear combination of the absorption spectra for **3′** and **4** is virtually indistinguishable from the absorption spectrum of model dyad **2′** with maxima at 645, 598, 559, 516, 428, 405(sh), 375(sh), and 312 nm.

**Fluorescence Emission.** The fluorescence emission spectra of **2**, **3**, and **4** with the same absorbance at the excitation wavelength of 520 nm, in tetrahydrofuran, are shown in Figure 2a. The emission spectra feature maxima for the dimesitylporphyrin at 650 and 718 nm and for the fluorinated porphyrin at 646 and 713 nm. The fluorescence of **2** has maxima at 649 and 717 nm.

The fluorescence emission spectra of **2′**, **3′**, and **4** dissolved in tetrahydrofuran and having the same absorbance at the excitation wavelength of 580 nm are shown in Figure 2b. The emission spectra feature maxima for the dimesityl zinc porphyrin at 604 and 655 nm. The emission of **2′**, with maxima at 651 and 713 nm, is reduced compared to that of **3′** and **4**, suggesting that the excited singlet states of the porphyrin moieties in **2′** are quenched by some photochemical process(es).

**Time-Resolved Fluorescence.** To learn more about the nature of the fluorescence quenching, time-resolved fluorescence experiments were undertaken, at room temperature, using the single-photon-timing technique. A tetrahydrofuran solution of model dyad **2** was excited at 625 nm, and the fluorescence decay was measured at seven wavelengths in the 600−800 nm region. Global analysis of these data ($\chi^2 = 1.15$) yielded two significant

**CHART 1**

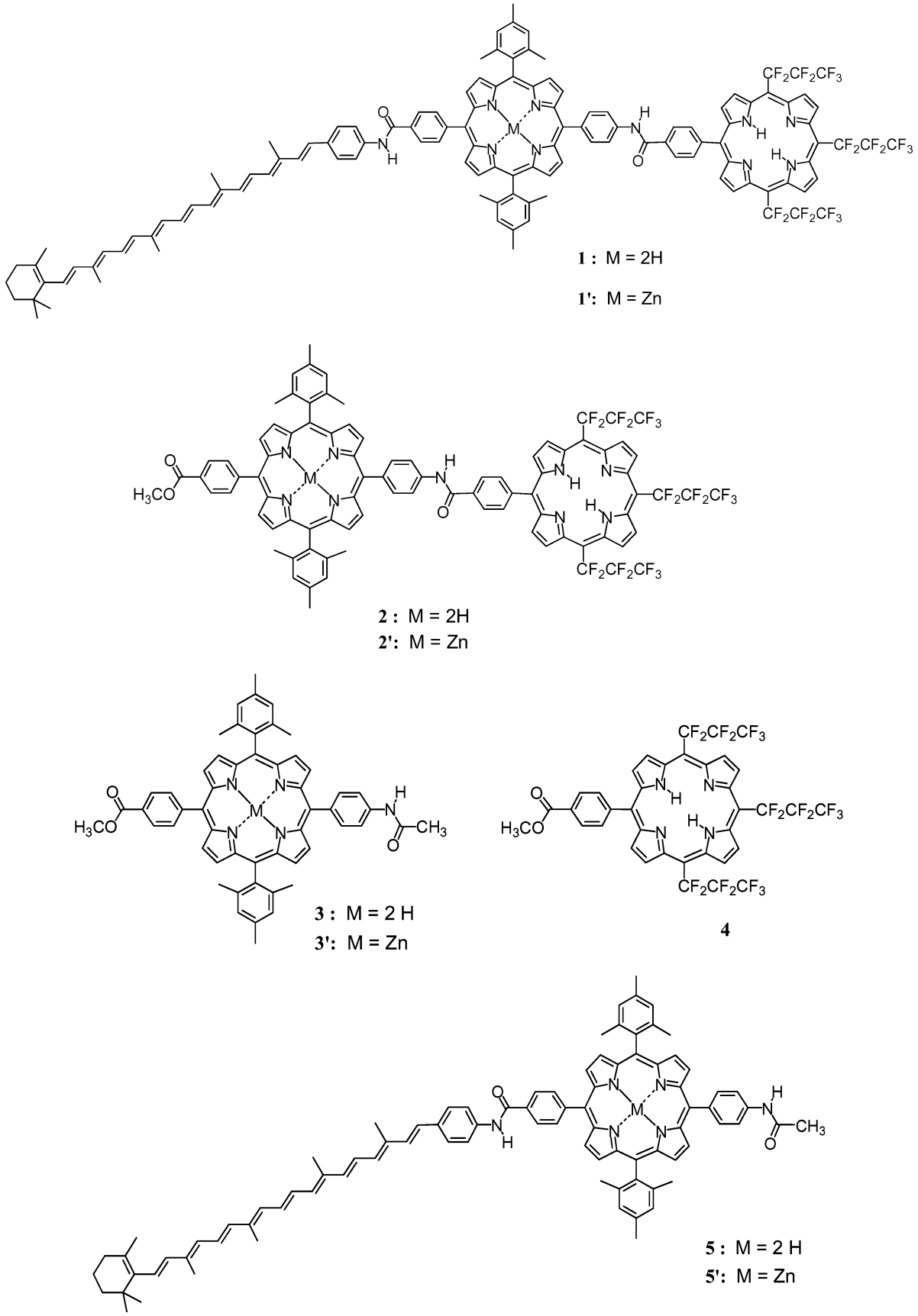


decay components with lifetimes of 12 and 890 ps (the relative amplitudes were wavelength dependent (60% and 35%) at the fluorescence maximum, respectively). Additional components with lifetimes of 0.12 and 11.5 ns (≤5% of the decay) were also required to fit the data; those were ascribed to minor impurities. Similar results were obtained with triad **1**, with two major decay components of 12 and 785 ps ($\chi^2 = 1.19$) and minor components of 0.14 and 11.5 ns (<5% of the decay), most likely

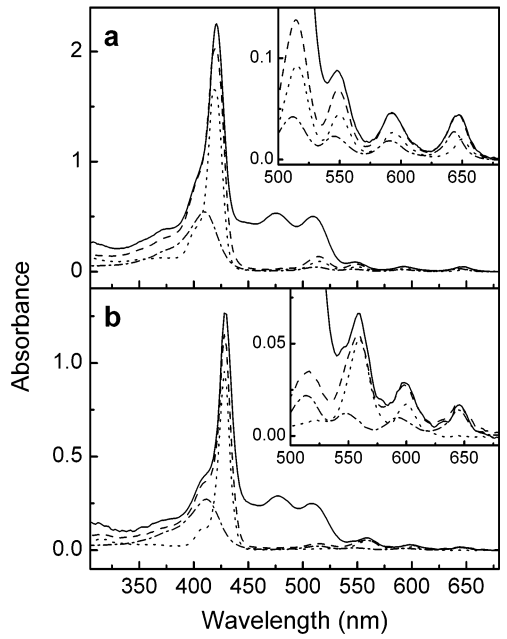


**Figure 1.** (a) Absorption spectra in tetrahydrofuran of triad **1** (——), model dyad **2** (---), model porphyrin **3** (·····), and model porphyrin **4** (-·-·-). (b) Absorption spectra in tetrahydrofuran of triad **1′** (——), model dyad **2′** (---), model porphyrin **3′** (·····), and model porphyrin **4** (-·-·-). The insets are expansions of the Q-band absorption region.

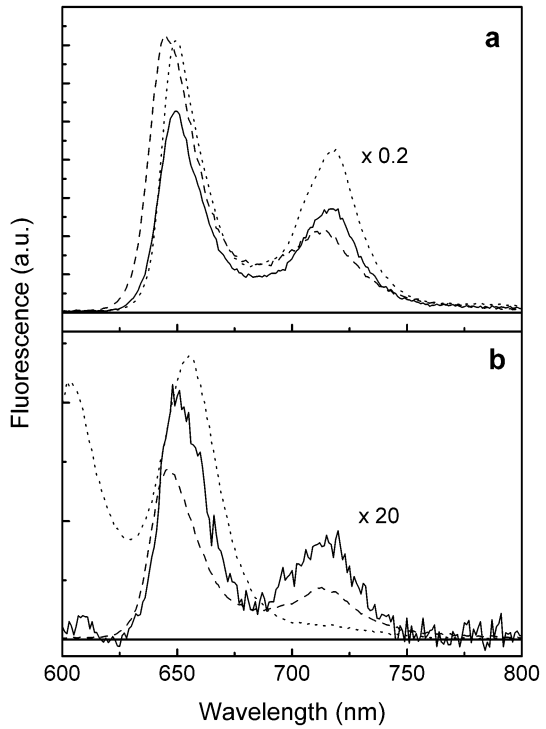


**Figure 2.** (a) Fluorescence emission spectra in tetrahydrofuran solution of dyad **2** (——), model porphyrin **3** (·····), and model porphyrin **4** (---) with excitation at 520 nm. The fluorescence of **4** has been multiplied by 0.2. (b) Fluorescence emission spectra in tetrahydrofuran solution of dyad **2′** (——), model porphyrin **3′** (·····), and model porphyrin **4** (---) with excitation at 580 nm. The fluorescence of **2′** has been multiplied by 20.

due to impurities. The fluorescence lifetimes for model porphyrins **4** and **3**, in tetrahydrofuran solution, were found to be 2.06 ns ($\chi^2 = 1.09$) and 11.50 ns ($\chi^2 = 1.13$), respectively. The fluorescence lifetimes of the dimesitylporphyrin in model dyad **5**, in tetrahydrofuran and benzonitrile, were found to be 3.27 ns ($\chi^2 = 1.19$) and 770 ps (additional 2.2 and 12.2 ns components <8% of the decay were required, $\chi^2 = 1.06$), respectively. The spectra of the major decay components are consistent with the steady-state fluorescence spectra of the model porphyrins. The significant shortening of the lifetime of the singlet states of the porphyrins in dyad **2** relative to that of the corresponding states in the model porphyrins is ascribed to excited-state energy exchange and photoinduced electron transfer (vide infra).

**TABLE 1: Excited Singlet State Lifetimes[a] of Porphyrin Moieties As Determined by Time-Resolved Fluorescence Studies[b]**

| compd | $\tau_1$ (ns) | $\tau_2$ (ns) |
|---|---|---|
| **1** | 0.012 | 0.785 |
| **2** | 0.012 | 0.890 |
| **3** | 11.50 | |
| **4** | 2.06 | |
| **5** | 3.27 (0.770)[c] | |
| **2′** | 0.013 (0.049)[d] | 0.040 (2.52)[d] |
| **3′** | 2.27 | |
| **5′** | 0.590 (0.370)[c] | |

[a] All lifetimes were determined in tetrahydrofuran unless otherwise noted. [b] In some cases, minor decay components were also observed (see text for details). [c] In benzonitrile. [d] In *n*-hexane.

Tetrahydrofuran and *n*-hexane solutions of model dyad **2′** were excited at 590 nm, and the fluorescence decay was measured at three wavelengths in the 600−800 nm region. Global analysis of the data ($\chi^2 = 1.17$) yielded two significant decay components with lifetimes of 13 and 40 ps for the tetrahydrofuran solution (the relative amplitudes were wavelength dependent, at 600 nm 99% of 13 ps and at 720 nm 25% of 13 ps and 75% of 40 ps) and 49 ps and 2.52 ns for the *n*-hexane solution (the relative amplitudes were wavelength dependent, at 600 nm 98% of 49 ps and at 720 nm 7% (negative amplitude) of 49 ps and 90% of 2.52 ns). Additional components with amplitude less than 3% were also required to fit the data; those were ascribed to minor impurities. In both solvents, the major decay component at 600 nm corresponds to emission from the zinc porphyrin, while the major decay component at 720 nm corresponds to emission from the free base fluorinated porphyrin.

Model porphyrin **3′** and model dyad **5′** in tetrahydrofuran showed fluorescence lifetimes of 2.27 ns ($\chi^2 = 1.05$) and 590 ps (additional 1.95 ns component <9% of the decay was required, $\chi^2 = 1.00$), respectively. The fluorescence lifetime of dyad **5′** in benzonitrile is quenched to 370 ps (additional 0.9 and 2.1 ns components <10% of the decay were required, $\chi^2 = 1.10$). It is well-known that the attachment of carotenoid moieties to porphyrins quenches the porphyrin singlet lifetime, possibly due to singlet energy and/or electron transfer between the chromophores (vide infra).

Transient fluorescence data for **1** and model compounds are compiled in Table 1.

**Time-Resolved Absorption.** Transient absorption experiments were undertaken in order to characterize the various excited states in these compounds and to allow detection of nonemissive species such as charge-separated states.

Solutions of **1**, **1′**, **2**, **2′**, **5**, and **5′** in tetrahydrofuran were excited with ~100 fs laser pulses, and the transient absorptions were recorded using the pump−probe method. The spectra were measured in the 930−1070 nm and 450−760 nm regions. A total of 70 and 155 kinetic traces were recorded over those wavelength regions, respectively, at times ranging from −50 to 4500 ps relative to the laser flash. The data were fitted globally using singular value decomposition.[31,32]

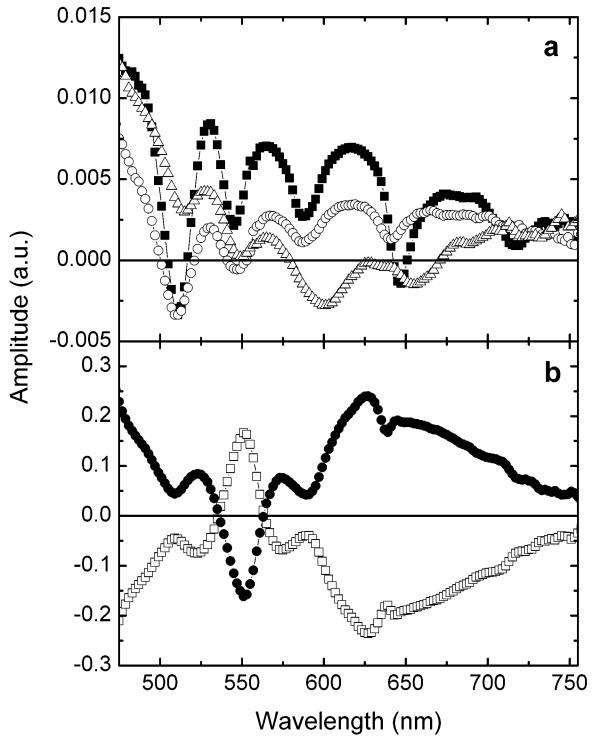


**Figure 3.** (a) Decay-associated spectra for **2** in tetrahydrofuran obtained from a global analysis of the transient absorption data taken after excitation at 550 nm with a ~100 fs laser pulse. The lifetimes of the components are 11.5 ps (△), 890 ps (■), and ~4.2 ns (○). (b) Decay-associated spectra for **2′** in tetrahydrofuran obtained from a global analysis of the transient absorption data taken after excitation at 645 nm. The lifetimes of the components are 40 ps (□) and 70 ps (●).

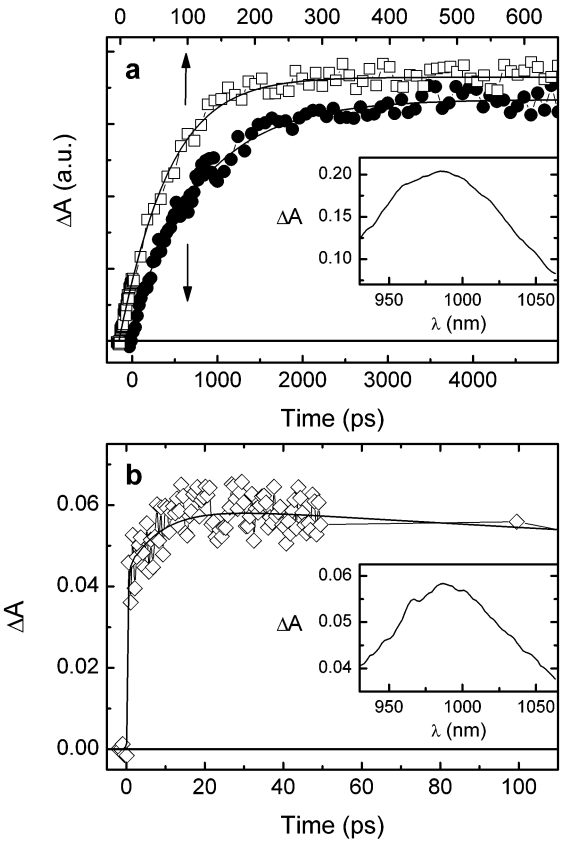


**Figure 4.** (a) Transient absorption kinetics at 980 nm measured for tetrahydrofuran solutions of triads **1** (●) and **1′** (□) with excitation by a ~100 fs laser pulse at 590 and 645 nm, respectively. A two-exponential fit to the data of triad **1** with time constants of 820 ps and a fixed, nondecaying component is shown as a smooth curve. A three-exponential fit to the data of triad **1′** with time constants of 40, 60 ps and a fixed, nondecaying component is shown as a smooth curve (arrows indicate corresponding time axes). The inset shows the transient absorption spectrum measured 4 ns after excitation of triad **1′** at 645 nm. (b) Transient absorption kinetics at 980 nm measured for a benzonitrile solution of dyad **5** with excitation at 600 nm. A two-exponential fit to the data of dyad **5** with time constants of 7 and 770 ps is shown as a smooth curve. The inset shows the transient absorption spectrum measured 50 ps after excitation.

Verification of the formation of a $P^{\bullet+}-P_F^{\bullet-}$ charge-separated state comes from the spectroscopic investigation of dyad **2** with excitation at 550 nm. Figure 3a shows the decay-associated spectra of dyad **2** obtained by a global analysis of the data. The best fit was achieved with three components having lifetimes of 11.5 ps, 890 ps, and ~4.2 ns.[33] The picosecond components have characteristic porphyrin ground-state bleaching at ~510, 550, 590, and 650 nm and stimulated emission bands at ~650 and 720 nm. They are consistent with an equilibration process mediated by singlet−singlet energy transfer between the two porphyrins, and subsequent formation of the $P^{\bullet+}-P_F^{\bullet-}$ charge separated state. The nanosecond component shows spectral characteristics of the porphyrin radical cation and anion[34,35] with ground-state bleaching bands; stimulated emission was not observed on the nanosecond time scale.

Formation of the $P_{Zn}^{\bullet+}-P_F^{\bullet-}$ charge-separated state was corroborated by spectroscopic investigation of dyad **2′** with excitation at 645 nm. This light selectively excites $P_F$ of dyad **2′**. Figure 3b shows the decay-associated spectra of dyad **2′** obtained by a global analysis of the data. The best fit was obtained with two components, 40 and 70 ps. The spectra are consistent with the decay of the initially formed $P_F$ singlet excited state in 40 ps and formation of the $P_{Zn}^{\bullet+}-P_F^{\bullet-}$ charge-separated state, which consequently decays to the ground state with a 70 ps lifetime. The 70 ps component clearly shows a broad induced absorption band at ~650 nm associated with $P_{Zn}^{\bullet+}$ and a ground-state bleaching band at 560 nm corresponding to $P_{Zn}$.

Figure 4a (circles) presents the kinetics obtained at 980 nm by excitation of triad **1** in solution with a 590 nm laser pulse. This light is absorbed mainly by the porphyrin moieties. Over time, a new transient species grows in with an absorbance maximum at ~980 nm, which is ascribed to the carotenoid radical cation. When the spectrum is monitored at 980 nm, the carotenoid radical cation absorption is found to appear with an 820 ps time constant. The carotenoid radical cation absorption band does not decay over a period of 4.5 ns, which is the longest time scale available on the spectrometer.

Figure 4a (squares) shows the results obtained from excitation of triad **1′** in tetrahydrofuran solution with a 645 nm laser pulse. This light, as mentioned before, is absorbed only by the fluorinated porphyrin moiety. Over time, in this case also, a new transient species grows in with an absorbance maximum at ~980 nm (inset Figure 4a), which is ascribed to the carotenoid radical cation. When the spectrum is monitored at 980 nm, the carotenoid radical cation absorption is found to grow in (negative amplitude) with a 60 ps time constant. An additional time constant of 40 ps (positive amplitude) due to decay of the fluorinated porphyrin singlet excited state (vide infra) also was needed to fit the kinetic results. The carotenoid radical cation absorption band does not decay on the longest time scale available to the spectrometer (4.5 ns).

The formation of $C^{\bullet+}-P^{\bullet-}-P_F$ and $C^{\bullet+}-P_{Zn}^{\bullet-}-P_F$ charge-separated states or singlet energy transfer from the porphyrin

to the carotenoid moiety as quenching mechanisms for P or $P_{Zn}$ excited singlet states was investigated by studying model dyads **5** and **5′**. No evidence of either process was observed in tetrahydrofuran solution. Nevertheless, the formation of short-lived $C^{\bullet+}-P^{\bullet-}$ or $C^{\bullet+}-P_{Zn}^{\bullet-}$ charged-separated states cannot be ruled out, because the formation of such states is energetically favorable in both cases and the fluorescence lifetime of the porphyrin is much more quenched in polar solvents, suggestive of electron-transfer processes.[36] It is possible that slow formation and a very short lifetime of the $C^{\bullet+}-P^{\bullet-}$ or $C^{\bullet+}-P_{Zn}^{\bullet-}$ charge-separated states precludes the build up of sufficient concentration to be observed by transient absorption spectroscopy. An alternative explanation for the porphyrin fluorescence lifetime quenching would be energy transfer to the carotenoid or an increase of the rate constant for internal conversion to the ground state and/or intersystem crossing, caused by the carotenoid moiety.

To investigate electron transfer as a mechanism for the fluorescence quenching of the porphyrin, dyads **5** and **5′** were studied in the polar solvent benzonitrile. Figure 4b (diamonds) presents the kinetics obtained at 980 nm by excitation of dyad **5** with a 650 nm laser pulse (a similar result was observed with dyad **5′** and excitation at 605 nm). This light was absorbed mainly by the porphyrin moiety. A new transient species grows in with an absorbance maximum at ~980 nm (inset in Figure 4b), which is ascribed to the carotenoid radical cation of $C^{\bullet+}-P^{\bullet-}$. When the spectrum was monitored at 980 nm, the carotenoid radical cation absorption was found to rise in with a 7 ps time constant and decay over a period of 770 ps. This observation is in agreement with time-resolved fluorescence results for **5** provided that the rise of the charge-separated state (770 ps) is slower than its decay (7 ps). In the case of the metalated dyad **5′**, the signal at 980 nm rises with a 20 ps time constant and decays in 370 ps**.** This observation illustrates that quenching of the porphyrin excited state in porphyrin−carotenoid dyads **5** and **5′** can be explained by the formation of a very short lived charge-separated state.

Excitation of deoxygenated samples of **1** and **1′** in tetrahydrofuran with a ~5 ns laser pulse at 590 nm permitted further investigations of the fate of the long-lived charge-separated state. Figure 5 presents the kinetics and spectra (see insets) of the carotenoid radical cation (a) and the carotenoid triplet excited state with a maximum at ~540 nm (b). An exponential fit to the kinetics at 980 nm yielded time constants of 500 ns and 210 ns for triads **1** and **1′**, respectively. A minor (<5%) long component of tens of microseconds was also required to fit the data. This minor decay component was sensitive to the presence of oxygen and therefore can be attributed to triplet states. Exponential fits to the kinetics at 540 nm for triads **1** and **1′** gave the corresponding 500 and 210 ns rise times, respectively, and a 4.9 $\mu$s decay component in both cases. Thus, the charge recombination process of $C^{\bullet+}-P-P_F^{\bullet-}$ and $C^{\bullet+}-P_{Zn}-P_F^{\bullet-}$ result in population of the carotenoid triplet excited state (vide infra).

**Quantum Yields.** Using the comparative method and 5,10,15,20-tetrakis(4-methylphenyl)porphyrin as a standard ($\epsilon_{T-G}$, 450 nm = $6.8 \times 10^4$ $M^{-1}$ $cm^{-1}$, $\Phi_T = 0.67$),[37,38] the quantum yields of the final charge separated states in triads **1** and **1′** were determined as 0.73 and 0.14, respectively, based on the absorption of the carotenoid radical cation ($\epsilon_{C^{\bullet+}}$, 950 nm = $1.6 \times 10^5$ $M^{-1}$ $cm^{-1}$). Using the same porphyrin as a standard, the quantum yield of the carotenoid triplet ($\epsilon_{T-G}$, 540 nm = $1 \times 10^5$ $M^{-1}$ $cm^{-1}$) in triads **1** and **1′** was determined to be 0.85 and 0.06, respectively, at room temperature.

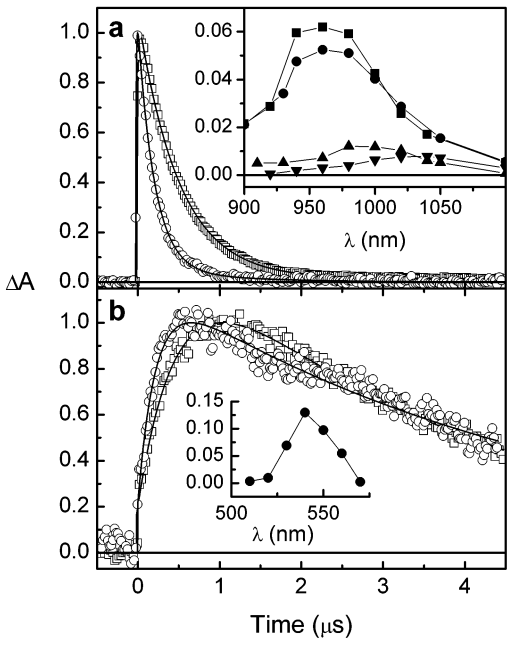


**Figure 5.** Normalized transient absorption kinetics measured for triads **1** (□) and **1′** (○) in deoxygenated tetrahydrofuran (room temperature) at 980 nm (a) and 540 nm (b), following excitation with a 5 ns, 590 nm laser pulse. In part (a), a two-exponential fit to the data is shown as a smooth curve with time constants of 500 ns (triad **1**) and 210 ns (triad **1′**) (in each case a minor component, <5%, of tens of microseconds was used). In part (b), a two-component fit to the data is shown as a smooth curve with time constants for the rise of 500 ns (triad **1**) and 210 ns (triad **1′**) and a decay time constant of 4.9 $\mu$s in both cases. The inset in part (a) shows the transient absorption spectra of **1** (**1′** is similar) 45 ns after the laser flash in 2-methyltetrahydrofuran at different temperatures (the carotenoid radical cation maximum is at ~980 nm): 300 K (■), 200 K (●), 105 K (▲), and 77 K (▼). The inset in part (b) shows the transient absorption spectrum taken 900 ns after the laser pulse (at room temperature), which is characteristic of the carotenoid triplet excited state (maximum at ~540 nm) of **1** (**1′** is similar).

**Low-Temperature Measurements.** Excitation of deoxygenated samples of **1** (Figure 6a) and **1′** (Figure 6b) in 2-methyltetrahydrofuran at temperatures between 300 and 77 K with a ~5 ns laser pulse at 532 nm permitted investigation of the fate of the long-lived charge-separated state at low temperatures.

For both triads, the decay kinetics are essentially single exponential above ~120 K (gray circles in Figure 6). From room temperature to ~250 K, charge recombination in $C^{\bullet+}-P_{Zn}-P_F^{\bullet-}$ is an activated process with an Arrhenius activation energy of ~0.23 eV (see Figure 6b). From 250 to ~120 K, the rates for triads **1** and **1′** are similar and almost independent of temperature. At around the glass transition temperature of 2-methyltetrahydrofuran (120−105 K) and below, the decay of the transient absorption displays two major exponential rate constants, $k_a$ and $k_b$ (gray and white circles in Figure 6) with amplitudes $a_a$ and $a_b$. The amplitude of the longer component, $a_b$, is one-half to one-third that of the shorter component over the range of 120−105 K and becomes much smaller as the temperature decreases to 77 K. This complex decay can be ascribed to heterogeneity in the organic glass and/or aggregation of the sample. Below ~120 K, the transient absorption spectra of the triads are perturbed in the carotenoid radical cation absorption region (shift to longer wavelengths) due to an apparent emission (maximum at ~960 nm), which may arise from molecular aggregates formed at these temperatures (see inset in Figure 5a). The amplitudes of the spectra presented in

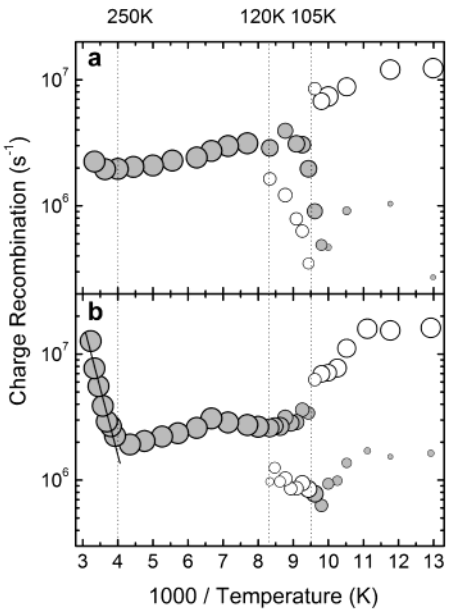


**Figure 6.** Temperature dependence of the final charge separated state decay in triads **1** (a) and **1′** (b) in 2-methyltetrahydrofuran after excitation with 5 ns laser pulses at 532 nm. Two major rate constants, shown as gray and white circles, were obtained from a three-exponential fit to the data. For both triads at all temperatures a long-lived component (100 $\mu$s, <5%) was fixed as the third exponential to improve the fit. Above 120 K, the kinetics are essentially single exponential (minor components, <5%, are not shown). The areas of the symbols indicate the relative amplitudes at each temperature. The straight line in (b) shows the Arrhenius fit (activation energy 0.23 eV) to the data for **1′** at higher temperatures (>250 K).

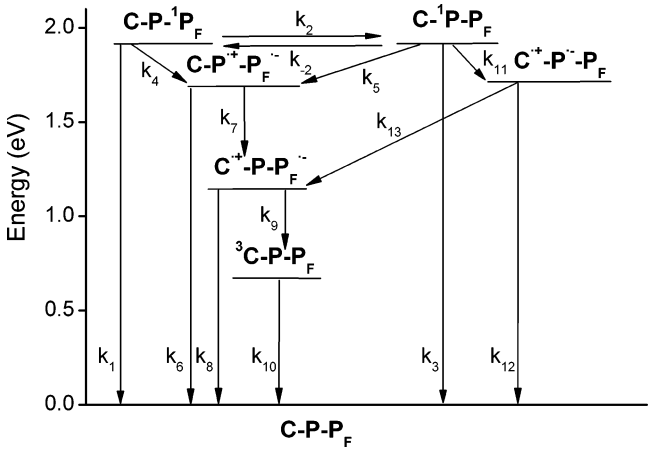


**Figure 7.** Transient states of triad **1** and relevant interconversion pathways. The energies of the various states have been estimated as discussed in the text, and no correction for Coulombic effects on the energies of the charge-separated states has been made.

Figure 5a illustrate the substantial decrease in quantum yield of the final charge-separated state as the temperature is lowered.

## Discussion

**Analysis of the Kinetic Data.** *C−P−P$_F$, Triad 1.* The model chosen for the interpretation of the kinetic and spectroscopic data dealing with singlet energy and electron transfer in triad **1** is shown in Figure 7, which indicates the relevant high-energy states and kinetic pathways. The energies of the various spectroscopic states were determined from the wavenumber average of the longest wavelength absorption and shortest wavelength emission maxima of **1** and appropriate model compounds. The fluorinated porphyrin first excited singlet state lies at 1.92 eV, whereas the energy of $C-{}^1P-P_F$ is 1.91 eV above the ground state. The energies of the $C-P^{\bullet+}-P_F^{\bullet-}$, $C^{\bullet+}-P^{\bullet-}-P_F$, and $C^{\bullet+}-P-P_F^{\bullet-}$ charge-separated states were estimated from cyclic voltammetric data described above. The energy of the triplet state $^3C-P-P_F$ of **1** is not known; but the energy of the lowest triplet state of a closely related carotenoid has been estimated to be 0.63 eV.[39] The difference in energy between the porphyrin first excited singlet states of triad **1** is only 0.01 eV. Thus, the equilibrium constant ($K$) for singlet−singlet energy transfer is 1.5 at ambient temperatures. If singlet−singlet energy transfer (steps 2 and −2) occurs at rates comparable to or greater than those of the other steps shown in Figure 7, both excited states will be significantly populated during the decay process. The general solution for coupled reactions of this type reveals that two fluorescence lifetimes or two components from transient absorption data are to be expected for the decay of the two excited singlet states.[40] As mentioned above, two significant fluorescence lifetimes were observed with triad **1** (12 and 785 ps) and dyad **2** (12 and 890 ps). The corresponding components from the transient absorption measurements with dyad **2** were 11.5 and 890 ps (Figure 3a). The reciprocals of these lifetimes ($\gamma_1$ and $\gamma_2$) do not represent any of the rate constants in the scheme. Rather

$$\gamma_1 = \{(X + Y) + [(X - Y)^2 + 4k_2k_{-2}]^{1/2}\}/2 \quad (1)$$

$$\gamma_2 = \{(X + Y) - [(X - Y)^2 + 4k_2k_{-2}]^{1/2}\}/2 \quad (2)$$

where

$$X = k_1 + k_5 + k_2 \quad (3)$$

$$Y = k_3 + k_4 + k_{-2} \quad (4)$$

The quantities $\gamma_1 = 8.3 \times 10^{10}$ s$^{-1}$ (12 ps) and $\gamma_2 = 1.1 \times 10^9$ s$^{-1}$ (890 ps) are known from the fluorescence decay or transient absorption results of **2**. The rate constants $k_1$ and $k_3$ may be estimated from the fluorescence lifetimes of model compounds **4** and **3** as $k_1 = 4.9 \times 10^8$ s$^{-1}$ and $k_3 = 8.7 \times 10^7$ s$^{-1}$, respectively. The equilibrium constant for the singlet-energy transfer between the porphyrins, $K$, gives $k_{-2}$ as $k_2$/1.5. Thus, one is left with two equations and three unknowns ($k_2$, $k_4$, and $k_5$). Setting $k_5 = Bk_4$ allows one to derive an analytical solution in quadratic form

$$k_{-2} = \frac{-b \pm (b^2 - 4ac)^{1/2}}{2a} \quad (5)$$

where

$$a = 4[(K - B)^2 + (B + 1)^2K] \quad (6)$$

$$b = 4(K - B)[(B - 1)(\gamma_1 + \gamma_2) + 2(k_1 - Bk_3)] \quad (7)$$

$$c = [(B - 1)(\gamma_1 + \gamma_2) + 2(k_1 - Bk_3)]^2 - (B + 1)^2(\gamma_1 - \gamma_2)^2 \quad (8)$$

The $k_2$ and $k_{-2}$ values are essentially independent of $B$, with $k_2 = 5.3 \times 10^{10}$ s$^{-1}$ and $k_{-2} = 3.5 \times 10^{10}$ s$^{-1}$. Molecular orbital calculations (Hartree−Fock/STO-G3, Gaussian 98 and DFT, Siesta) were used to compare the amplitudes of the HOMO−HOMO (for hole transfer, step 4) and LUMO−LUMO (for electron transfer, step 5) orbitals at the meso positions linking P to P$_F$. Qualitatively, the amplitudes are similar. Thus, it is reasonable to assume that the electronic coupling is comparable for both reactions. In addition, there is only a small difference

in thermodynamic driving force for reactions 4 and 5, suggesting that the approximation $B = 1$ and $k_4 = k_5$ is reasonable. If this assumption is made, the above equations yield $k_4 = k_5 = 1 \times 10^9$ s$^{-1}$. This is consistent with results from studies of a series of porphyrin−porphyrin dyads related to **2**.[25]

On the basis of the transient absorption results for model compound **2** (Figure 3a), the excited states of the porphyrins are quenched by electron/hole transfer to produce $P^{\bullet+}-P_F^{\bullet-}$, which decays to the ground state with a ~4.2 ns time constant, so $k_6 \approx 1/4.2$ ns $= 2.4 \times 10^8$ s$^{-1}$. The charge shift rate $k_7$ for the formation of $C^{\bullet+}-P-P_F^{\bullet-}$ in triad **1** (Figure 4 circles) is not observed experimentally, because $k_7 \gg k_4$ or $k_5$, so the induced absorption rise at 980 nm is a single exponential with a lifetime associated with the formation of $C-P^{\bullet+}-P_F^{\bullet-}$ rather than $C^{\bullet+}-P-P_F^{\bullet-}$. The quantum yield of $C^{\bullet+}-P-P_F^{\bullet-}$, obtained using the comparative method (vide supra) is 0.73.[37,38] On the basis of this value, and assuming that $C^{\bullet+}-P^{\bullet-}-P_F$ decays only to the ground state and does not form $C^{\bullet+}-P-P_F^{\bullet-}$, the kinetic scheme requires that $k_7 \geq 1 \times 10^{10}$ s$^{-1}$. (Note that for $k_7 > 10^{10}$ s$^{-1}$ the quantum yield is a weak function of the value of $k_7$. In a related triad, $C-P-C_{60}$, having the same carotenoid and porphyrin moieties and linkage between them, we measured a rate constant for the charge shift equivalent to step 7 of $8.3 \times 10^9$ s$^{-1}$).[41] In principle, steps 11 and 13 in Figure 7 could also contribute to formation of $C^{\bullet+}-P-P_F^{\bullet-}$. Fluorescence quenching of the proximal porphyrin by the attached carotenoid is indicated as electron-transfer process 11 in Figure 7. A value for the rate constant $k_{11}$ of $2.2 \times 10^8$ s$^{-1}$ can be determined from the fluorescence lifetime of the porphyrin moiety of **5** (3.27 ns). Kinetic simulations show that if steps 11 and 13 occur, they could account for at most a 2% increase in the quantum yield of $C^{\bullet+}-P-P_F^{\bullet-}$. Experimentally it is not possible to observe step 13 because, like in the case of step 7, it is much faster than steps 4, 5, and 11.

The final charge recombination process is dominated by population of the carotenoid triplet excited state rather than direct recovery of the singlet ground state. From the flash photolysis results we know that the lifetime of $C^{\bullet+}-P-P_F^{\bullet-}$ is 500 ns (Figure 5a). Assuming that $k_8 \ll k_9$ would yield $k_9 = 2.0 \times 10^6$ s$^{-1}$. The carotenoid triplet state decays to the ground state with a rate constant $k_{10} = 2.0 \times 10^5$ s$^{-1}$ (from its lifetime of 4.9 $\mu$s).

*C−P$_{Zn}$−P$_F$, Triad 1′.* Figure 8 presents an energy level diagram showing the pertinent high-energy states and kinetic pathways used to interpret the kinetic and spectroscopic data dealing with singlet energy and electron transfer in triad **1′**. The fluorinated porphyrin first excited singlet state lies at 1.92 eV, whereas the energy of $C-{}^1P_{Zn}-P_F$ is 2.06 eV above the ground state. The energies of the charge-separated states were determined from the electrochemical measurements given above. The energy of the triplet state ${}^3C-P_{Zn}-P_F$ of **1′** is the same as that of the corresponding state in **1**.

Rate constants $k_1$ and $k_3$ may be estimated from the fluorescence lifetimes of model compounds **4** and **3′**; $k_1 = 4.9 \times 10^8$ s$^{-1}$ and $k_3 = 4.4 \times 10^8$ s$^{-1}$. On the basis of the transient absorption results for model compound **2′**, the fluorinated porphyrin singlet excited state is quenched to 40 ps by hole transfer to produce $P_{Zn}^{\bullet+}-P_F^{\bullet-}$, which decays to the ground state with a 70 ps time constant (Figure 3b). Therefore, the rate constants $k_5$ and $k_6$ can be estimated as $k_5 = 2.5 \times 10^{10}$ s$^{-1}$ [assuming $k_5 =$ (1/40 ps) $- k_1$] and $k_6 = 1/70$ ps $= 1.43 \times 10^{10}$ s$^{-1}$. On the basis of the fluorescence lifetime measurements for model dyad **2′**, the zinc porphyrin excited singlet state is quenched to 13 ps by a combination of singlet−singlet energy transfer and electron transfer to produce the $P_{Zn}^{\bullet+}-P_F^{\bullet-}$ state. Assuming that energy transfer to $P_F$ dominates the relaxation of ${}^1P_{Zn}-P_F$ in *n*-hexane and that the energy transfer rate in *n*-hexane is nearly equal to that in tetrahydrofuran, $k_2 \sim 2.0 \times 10^{10}$ s$^{-1}$ [$k_2 =$ (1/49 ps) $- k_3$]. This allows the calculation of $k_4 \approx 5.5 \times 10^{10}$ s$^{-1}$ [$k_4 =$ (1/13 ps) $- k_3 - k_2$].

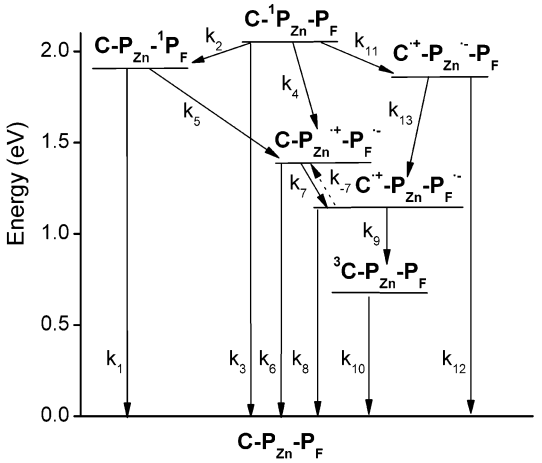


**Figure 8.** Transient states of triad **1′** and relevant interconversion pathways. The energies of the various states have been estimated as discussed in the text, and no corrections for Coulombic effects on the energies of the charge-separated states have been made. The dotted arrow shows a pathway of activated decay of the final charge-separated state at temperatures >250 K.

The charge shift rate $k_7$ for the formation of the final charge-separated state $C^{\bullet+}-P_{Zn}-P_F^{\bullet-}$ in triad **1′** can be estimated as $2.4 \times 10^9$ s$^{-1}$ from the relationship $k_7 =$ (1/60 ps) $- k_6$. This relationship is based on the rise of the carotenoid radical cation transient absorption signal at 980 nm, which displays 40 and 60 ps components (Figure 4). The 60 ps component is identified with the decay of $C-P_{Zn}^{\bullet+}-P_F^{\bullet-}$ because the 40 ps component matches the lifetime of $C-P_{Zn}-{}^1P_F$ (formation of $C-P_{Zn}^{\bullet+}-P_F^{\bullet-}$) as determined from fluorescence measurements. From the nanosecond flash photolysis results we know that the lifetime of the $C^{\bullet+}-P_{Zn}-P_F^{\bullet-}$ state is 210 ns (assuming that $k_8 \ll k_9$, $k_9 + k_{-7} = 4.8 \times 10^6$ s$^{-1}$, Figure 5a) at room temperature and that the quantum yield of formation of the carotenoid triplet state by charge recombination from the final charge separated state is about $\Phi \sim 0.06$ (vide supra). The carotenoid triplet state decays to the ground state with rate constant $k_{10} = 2.0 \times 10^5$ s$^{-1}$ (lifetime 4.9 $\mu$s).

As mentioned above, fluorescence quenching of the model porphyrin by the attached carotenoid in dyad **5′** is likely due to electron transfer from the carotenoid to the zinc dimesityl porphyrin. The rate constant for this quenching is $k_{11} = 1.3 \times 10^9$ s$^{-1}$.

The kinetic data described above are compiled in Table 2.

**Quantum Yields.** The quantum yields of $C-P^{\bullet+}-P_F^{\bullet-}$ and $C^{\bullet+}-P-P_F^{\bullet-}$ based on the excitation of the porphyrins may be determined by simulation of the kinetic pathways in Figures 7 and 8 using the rate constants given above. The simulations were done using Chemical Kinetics Simulator created by IBM, version 1.01 (see Experimental Section). Quantum yields of 0.73 for $C-P^{\bullet+}-P_F^{\bullet-}$ and 0.71 for $C^{\bullet+}-P-P_F^{\bullet-}$ were calculated. Similarly, quantum yields of 0.98 for $C-P_{Zn}^{\bullet+}-P_F^{\bullet-}$ and 0.14 for $C^{\bullet+}-P_{Zn}-P_F^{\bullet-}$ were calculated. The results of these simulations are in close agreement with the measured values of quantum yields by the comparative method (vide supra).

Because of the slow formation of the initial charge-separated state $C-P^{\bullet+}-P_F^{\bullet-}$ in the case of triad **1** ($k_4 = k_5 = 9.1 \times 10^8$

**TABLE 2: Kinetic Data and Quantum Yields for the Formation of Charge-Separated States at Room Temperature of C−P−$P_F$ (Triad 1) and C−$P_{Zn}$−$P_F$ (Triad 1′) in Tetrahydrofuran**

| rate constants $(ns)^{-1}$ | | | | | | | quantum yields | |
|---|---|---|---|---|---|---|---|---|
| Triad **1** | | | | | | | | |
| $k_1$ | $k_2$ | $k_{-2}$ | $k_3$ | $k_4$ | $k_5$ | $k_6$ | $\Phi_{C-P^{\bullet+}-P_F^{\bullet-}}$ | $\Phi_{C^{\bullet+}-P-P_F^{\bullet-}}$ |
| 0.49 | 53 | 35 | 0.087 | 1 | 1 | ∼0.24 | | |
| $k_7$ | $k_8$ | $k_9$ | $k_{10}$ | $k_{11}$ | $k_{12}$ | $k_{13}$ | 0.73 | 0.71 |
| ≥10 | $\ll k_9$ | 0.002 | 0.0002 | 0.22 | <143 | $\gg k_5$ | | |
| Triad **1′** | | | | | | | | |
| $k_1$ | $k_2$ | $k_3$ | $k_4$ | $k_5$ | $k_6$ | $k_7$ | $\Phi_{C-P_{Zn}^{\bullet+}-P_F^{\bullet-}}$ | $\Phi_{C^{\bullet+}-P_{Zn}-P_F^{\bullet-}}$ |
| 0.49 | ∼20 | 0.44 | ∼55 | 25 | ∼14.3 | 2.4 | | |
| $k_{-7}$ | $k_8$ | $k_9$ | $k_{10}$ | $k_{11}$ | $k_{12}$ | $k_{13}$ | 0.98 | 0.14 |
| ∼0.0023 | $\ll k_9$ | 0.002 | 0.0002 | 1.3 | <50 | $\gg k_5$ | | |

$s^{-1}$), a considerable amount of the observed carotenoid triplet (14%) is formed by triplet−triplet energy transfer from the triplet excited states of both porphyrins formed by normal intersystem crossing.[42] This accounts for the discrepancy between the quantum yield of formation of the final charge-separated state (73%) and the quantum yield of the carotenoid triplet produced (85%). In triad **1′**, the formation of the initial charge separation C−$P_{Zn}^{\bullet+}$−$P_F^{\bullet-}$ is much faster ($k_4 = 5.5 \times 10^{10}$ $s^{-1}$ and $k_5 = 2.5 \times 10^{10}$ $s^{-1}$) than in triad **1** ($k_4 = 1 \times 10^9$ $s^{-1}$ and $k_5 = 1 \times 10^9$ $s^{-1}$); thus, little porphyrin triplet is formed by normal intersystem crossing, so the carotenoid triplet is essentially all formed from recombination of the triplet radical pair state. However, above 250 K almost 50% of the final charge-separated state returns to the initial charge separated state (vide infra), which in turn rapidly decays mostly to the ground state. Thus the quantum yield of carotenoid triplet is 0.06, even though the yield of $C^{\bullet+}$−$P_{Zn}$−$P_F^{\bullet-}$ is 0.14. Time-resolved EPR measurements are underway to further investigate these findings.

**Charge Recombination of $C^{\bullet+}$−P−$P_F^{\bullet-}$ and $C^{\bullet+}$−$P_{Zn}$−$P_F^{\bullet-}$.** In 2-methyltetrahydrofuran, charge recombination has been measured in **1** and **1′** from room temperature to ∼77 K (Figure 6). At temperatures above ∼250 K, charge recombination in $C^{\bullet+}$−$P_{Zn}$−$P_F^{\bullet-}$ is an activated process with an Arrhenius activation energy of ∼0.23 eV. From 250 to 120 K, the rate is almost independent of temperature and similar to that of triad **1**, in which there is no evidence for an activated process.

In principle, the charge recombination step could involve either a one-step electron transfer, as indicated by step 9 in Figures 7 and 8, or a two-step process, whereby an electron would be transferred endergonically from the central porphyrin to the carotenoid cation radical, yielding C−$P^{\bullet+}$−$P_F^{\bullet-}$ (C−$P_{Zn}^{\bullet+}$−$P_F^{\bullet-}$) as an intermediate (see Figure 8, step −7). From the intermediate state recombination to the ground state would again compete with formation of the final charge-separated state. Such an activated, two-step pathway to the ground state has been observed in some carotenoporphyrin−quinone triads and porphyrin−pyromellitimide−$C_{60}$ triads.[43−45] In an activated, two-step recombination, the rate should be limited by the energy difference between the final charge-separated state and the higher energy C−$P^{\bullet+}$−$P_F^{\bullet-}$/C−$P_{Zn}^{\bullet+}$−$P_F^{\bullet-}$ state (see Figures 7, 8) plus any additional activation energy associated with the electron transfer. In the case of triad **1′**, cyclic voltammetric measurements locate C−$P_{Zn}^{\bullet+}$−$P_F^{\bullet-}$ ∼0.24 eV higher in energy than $C^{\bullet+}$−$P_{Zn}$−$P_F^{\bullet-}$, which is consistent with the activation Arrhenius energy of 0.23 eV measured for this molecule (see linear fit in Figure 6).

In the case of triad **1**, C−$P^{\bullet+}$−$P_F^{\bullet-}$ is ∼0.54 eV higher in energy than $C^{\bullet+}$−P−$P_F^{\bullet-}$ and therefore not accessible at room temperature (vide infra), precluding a two-step process. This suggests that the difference in recombination rate of the final charge-separated states of **1′** and **1** above ∼250 K is due to the operation of a two-step mechanism in addition to the single step recombination in the case of **1′**, but not in **1**. Indeed, the intercept of the Arrhenius plot in Figure 6, for triad **1′**, gives a value of $\sim 3 \times 10^{10}$ $s^{-1}$, which is consistent with the modest electronic coupling associated with the linkage between C and $P_{Zn}$. Simulations using measured rate constants ($k_6$, $k_7$, and $k_{10}$) and assuming that $k_9$ is $2 \times 10^6$ $s^{-1}$ result in a value of $\sim 2.3 \times 10^6$ $s^{-1}$ for $k_{-7}$ (the rate constant for the endergonic step) and quantum yields of 0.14 for $C^{\bullet+}$−$P_{Zn}$−$P_F^{\bullet-}$ and 0.06 for $C^3$−$P_{Zn}$−$P_F$, in good agreement with measured values. The lifetime of $C^{\bullet+}$−$P_{Zn}$−$P_F^{\bullet-}$ of 258 ns at 298 K obtained by the simulation is in reasonable agreement with the observed lifetime of $C^{\bullet+}$−$P_{Zn}$−$P_F^{\bullet-}$ of 210 ns.

Turning now to triad **1**, recall that the energy of C−$P^{\bullet+}$−$P_F^{\bullet-}$ is about ∼0.54 eV above that of $C^{\bullet+}$−P−$P_F^{\bullet-}$. Because the electronic coupling term associated with the carotenoid to porphyrin linkage should be similar in **1** and **1′**, the same preexponential factor found for **1′** can be used to calculate the expected rate for the two-step process in **1**. The minimum activation energy of 0.54 eV combined with a preexponential factor of $3 \times 10^{10}$ $s^{-1}$ limits the Arrhenius rate constant for recombination by the two-step mechanism to 22 $s^{-1}$ (lifetime 45 ms) at 298 K, a value much smaller than observed, and establishes that the two-step mechanism is not kinetically allowed in triad **1**. These calculations together with similar values of recombination rates at low temperatures for both **1** and **1′** argue against the multistep process for triads **1** and **1′** at low temperatures and support it for triad **1′** at elevated temperatures. Thus, a single-step recombination reaction mechanism is assigned for triad **1** and triad **1′** at <250 K.

The recombination rate of both triads changes abruptly around 120−105 K (see Figure 6), which is the glass transition temperature of 2-methyltetrahydrofuran (the solvent dielectric constant changes from 18.8 to 2.6).[46] The decay of $C^{\bullet+}$−P−$P_F^{\bullet-}$/$C^{\bullet+}$−$P_{Zn}$−$P_F^{\bullet-}$ is no longer a single exponential, possibly due to molecular heterogeneity and/or aggregation that occurs as the solvent becomes glassy. Because of the spectral shift (Figure 5a) and quenched lifetime, it is tempting to assign the short-lived (∼60−100 ns, high amplitude) decay component to the transient absorption signal from aggregated molecules. The long-lived component (∼1 $\mu$s, small amplitude) is consistent with decay of the final charge-separated state in nonaggregated triads responding to the change in dielectric constant at the glass transition temperature, which would likely move the recombination process further into the Marcus−Hush inverted region, thereby slowing the process. The quantum yield of the final charge-separated state at low temperatures is very low; nevertheless, charge separation at 77 K has been confirmed by independent time-resolved EPR measurements (unpublished results).

## Conclusions

Relatively simple models of photosynthetic reaction centers consisting of two porphyrins and a carotenoid covalently linked in series exhibit rather complex relaxation pathways following excitation of the porphyrin moieties. The rate constants of all major processes have been measured or estimated using photophysical measurements on simpler model compounds. To a first approximation, the electronic couplings through the linkages connecting the components are the same in **1** and **1′**, so differences in rate constants for analogous steps in **1** and **1′** are due to thermodynamic effects, including reorganization energy differences, as noted in previous studies.[25] A major difference between the triads is in the energies of the intermediate charge-separated states. Metalating the central porphyrin lowers the energy of $C-P_{Zn}^{\bullet+}-P_F^{\bullet-}$ 0.2 eV below that of $C-P^{\bullet+}-P_F^{\bullet-}$. This energy difference controls the dynamics and quantum yields in predictable ways.

Formation of the initial charge separated state $C-P_{Zn}^{\bullet+}-P_F^{\bullet-}$ in **1′** is more than an order of magnitude faster than in triad **1**, due to the higher driving force for a process in the Marcus normal region. Because this step is relatively slow and rate limiting in **1**, the rise time of the carotenoid radical cation absorbance is associated with the *formation* of $C-P^{\bullet+}-P_F^{\bullet-}$, whereas in **1′** the rise time of the carotenoid radical cation absorbance is associated with the *decay* of the analogous initial charge-separated species, $C-P_{Zn}^{\bullet+}-P_F^{\bullet-}$.

Triad **1** generates a long-lived charge-separated state with a relatively high quantum yield of 73% at room temperature; the yield is much lower, 14%, in triad **1′**. This decrease in quantum yield arises because lowering the energy of the intermediate $C-P_{Zn}^{\bullet+}-P_F^{\bullet-}$ compared with $C-P^{\bullet+}-P_F^{\bullet-}$ reduces the driving force and thereby slows the charge shift in **1′**, which occurs in the Marcus normal region and yields the long-lived charge-separated species $C^{\bullet+}-P_{Zn}-P_F^{\bullet-}$. The rate of recombination to the ground state from $C-P_{Zn}^{\bullet+}-P_F^{\bullet-}$ is increased because recombination is less inverted in **1′** than in the higher energy intermediate in **1**, $C-P^{\bullet+}-P_F^{\bullet-}$. In other words, in accordance with Marcus theory, the 0.20 eV shift in $C-P_{Zn}^{\bullet+}-P_F^{\bullet-}$ increases $k_6$ and decreases $k_7$, thus lowering the quantum yield of $C^{\bullet+}-P_{Zn}-P_F^{\bullet-}$.

The electron−hole recombination process whereby $C^{\bullet+}-P-P_F^{\bullet-}$ and $C^{\bullet+}-P_{Zn}-P_F^{\bullet-}$ relax features population of the carotenoid triplet excited-state rather than recovery to the singlet ground state. This is a rather unusual observation in artificial photosynthetic systems but is observed in natural reaction centers. Even though the energies of $C^{\bullet+}-P-P_F^{\bullet-}$ and $C^{\bullet+}-P_{Zn}-P_F^{\bullet-}$ are essentially the same, the rates of the recombination reactions for **1** and **1′** at room temperature are different, 500 and 210 ns in tetrahydrofuran, respectively. Also, the temperature dependence of the lifetimes of $C^{\bullet+}-P-P_F^{\bullet-}$ and $C^{\bullet+}-P_{Zn}-P_F^{\bullet-}$ is significantly different, implying different mechanisms in the two triads. Indeed, the charge recombination reaction follows a single-step mechanism for $C^{\bullet+}-P-P_F^{\bullet-}$ over the entire temperature range (300−77 K), while in the case of $C^{\bullet+}-P_{Zn}-P_F^{\bullet-}$ recombination occurs solely by a single-step process only at temperatures below ∼250 K, where it has approximately the same rate observed for $C^{\bullet+}-P-P_F^{\bullet-}$. The different mechanisms arise from the 0.2 eV energy difference between the intermediate charge-separated states in **1** and **1′**. At temperatures above ∼250 K, the low-lying $C-P_{Zn}^{\bullet+}-P_F^{\bullet-}$ intermediate available to $C^{\bullet+}-P_{Zn}-P_F^{\bullet-}$ controls the dynamics by providing an endergonic, activated step that operates in addition to the direct process. An activated step at higher temperature and a temperature independent process at low temperature are reminiscent of the behavior observed in other triads. The intermediate $C-P_{Zn}^{\bullet+}-P_F^{\bullet-}$ recombines directly to the ground state rather than to the $^3C-P_{Zn}-P_F$ state.

The quantum yield for the formation of the final charge-separated state in both triads is reduced considerably at lower temperatures, the decrease being abrupt at 120−105 K, which is the glass transition range of 2-methyltetrahydrofuran. But even at 77 K, the signal associated with the carotenoid radical cation can be detected. At this temperature in most quinone-based artificial reaction centers the photoinduced electron-transfer reaction does not occur.[47,48] On the other hand, photoinduced electron transfer in $C_{60}$-based systems is generally less sensitive to temperature effects than the systems described herein. This is consistent with the unusually low reorganization energy associated with $C_{60}$, so even as solvent motion is frozen out to give a low dielectric environment, the process is still in a favorable Marcus region.

The fact that these porphyrin- and carotenoid-based systems demonstrate photoinduced electron transfer at low temperatures and charge recombination to form triplet states demonstrates that such phenomena are characteristic not only of natural photosynthesis and porphyrin−fullerene molecules but also of other molecular constructs in which large delocalized $\pi$-electron systems lead to low reorganization energies and a weak dependence of the energy of the radical ions on the environment.

The added driving force for photoinduced electron transfer in the $C-P_{Zn}-P_F$ triad is useful to drive electron transfer in low dielectric environments such as the interior of artificial biological membranes. However, this added driving force comes with a penalty in quantum yield and lifetime of the final charge-separated species. The analysis of the energy and electron/hole transfer processes in **1** and **1′** illustrates the interplay between factors controlling electron-transfer rates that must be considered for optimal function of artificial reaction centers in various environments.

## Experimental Section

**Instrumental Techniques.** The $^1H$ NMR spectra were recorded on Varian Unity spectrometers at 300 or 500 MHz. Unless otherwise specified, samples were dissolved in deuteriochloroform with tetramethylsilane as an internal reference. Mass spectra were obtained on a matrix-assisted laser desorption/ionization time-of-flight spectrometer (MALDI-TOF). Ultraviolet−visible ground-state absorption spectra were measured on a Shimadzu UV2100U UV−vis spectrometer.

**Electrochemical Measurements.** Reduction and oxidation potentials were measured by cyclic voltammetry in a two-compartment glass cell, with a glassy carbon electrode as the working electrode, a Pt wire as counter electrode, and Ag/$AgNO_3$ as a reference electrode. Electrode potentials are expressed vs SCE using ferrocene as internal standard (ferrocene/ferrocenium potential vs SCE: 0.458 V). The electrolyte solution was 0.1 M tetra-*N*-butylammonium hexafluorophosphate in benzonitrile. Solutions were purged with nitrogen or argon prior to measurements, and an inert atmosphere was maintained thereafter. Cyclic voltammograms, at scan rates from 10 to 500 mV/s, were obtained with a Pine AFRDE4 potentiostat and an X−Y recorder, or a PAR 173 potentiostat, a PAR 175 universal programmer, and a computer with LabView software.

Steady-state fluorescence emission spectra were measured using a Photon Technology International MP-1 spectrophotometer and corrected. Excitation was produced by a 75 W xenon lamp and a single grating monochromator. Fluorescence was

detected at 90° to the excitation beam via a single grating monochromator and an R928 photomultiplier tube having S-20 spectral response and operating in the single-photon-counting mode.

Fluorescence decay measurements were performed on $\sim 1 \times 10^{-5}$ M solutions by the time-correlated single photon counting method. The excitation source was a cavity-dumped Coherent 700 dye laser pumped by a frequency-doubled Coherent Antares 76s Nd:YAG laser. Fluorescence emission was detected at a magic angle using a single grating monochromator and microchannel plate photomultiplier (Hamamatsu R2809U-11). The instrument response time was ca. 60−90 ps, as verified by scattering from Ludox AS-40. The spectrometer was controlled by software based on a LabView program from National Instruments.

Nanosecond transient absorption measurements were made with excitation from an Opotek optical parametric oscillator pumped by the third harmonic of a Continuum Surelight Nd:YAG laser. The pulse width was ~5 ns, and the repetition rate was 5 Hz. The detection portion of the spectrometer has been described elsewhere.[49]

Low-temperature measurements were performed using an Oxford Optistat$^{DN}$ liquid nitrogen-cooled optical cryostat equipped with an Oxford ITC 601 temperature controller (accuracy ±0.1 K).

The femtosecond transient absorption apparatus consists of a kilohertz pulsed laser source and a pump−probe optical setup. The laser pulse train was provided by a Ti:sapphire regenerative amplifier (Clark-MXR, Model CPA-1000) pumped by a diode-pumped CW solid-state laser (Spectra Physics, Model Millennia V). The typical laser pulse was 100 fs at 790 nm, with a pulse energy of 0.9 mJ at a repetition rate of 1 kHz. Most of the laser energy (85%) was used to pump an optical parametric amplifier (IR-OPA, Clark-MXR). The excitation pulse was sent through a computer-controlled optical delay line. The remaining laser output (15%) was focused into a 1 cm flowing water cell to generate a white light continuum. The continuum beam was further split into two identical parts and used as the probe and reference beams, respectively. The probe and reference signals were focused onto two separate optical fiber bundles coupled to a spectrograph (Acton Research, Model SP275). The spectra were acquired on a dual diode array detector (Princeton Instruments, Model DPDA-1024).[50]

To determine the number of significant components in the transient absorption data, singular value decomposition analysis[31,32] was carried out using locally written software based on the MatLab 5.0 program (MathWorks, Inc.) Decay-associated spectra were then obtained by fitting the transient absorption change curves over a selected wavelength region simultaneously as described by eq 9

$$\Delta A(\lambda,t) = \sum_{i=1}^{n} A_i(\lambda) \exp(-t/\tau_i) \qquad (9)$$

where $\Delta A(\lambda,t)$ is the observed absorption change at a given wavelength at time delay $t$ and $n$ is the number of kinetic components used in the fitting. A plot of $A_i(\lambda)$ versus wavelength is called a decay-associated spectrum and represents the amplitude spectrum of the $i$th kinetic component, which has a lifetime of $\tau_i$. Random errors associated with the reported lifetimes obtained from transient absorption measurements were typically ≤5%.

Simulations of the kinetic pathways were performed with the Chemical Kinetics Simulator, Version 1.01, created by IBM. It uses a stochastic method, based on reaction probabilities, to calculate the time history of a chemical system using the reaction mechanism and specified initial conditions. For more information, see www.almaden.ibm.com/st/computational_science/ck/msim/index.shtml.

**Synthesis.** All chemicals employed in the preparation of the following compounds were purchased from Aldrich, Acros, or Lancaster. Solvents were bought from EM Science. Tetrahydrofuran was distilled from sodium and benzophenone in a nitrogen atmosphere immediately prior to use. Toluene was distilled from $CaH_2$ and dichloromethane was distilled from calcium carbonate. All solvents were stored over the appropriate molecular sieves. Pyrrole was distilled prior to use. For thin-layer chromatography (TLC), silica gel coated glass plates from Analtech were used. Column chromatography was carried out using EM Science silica gel 60 with 230−400 mesh. Unless otherwise specified, all reactions were carried out under a nitrogen atmosphere. 5-Mesityldipyrromethane (**6**), 5,15-bis(4-carbomethoxyphenyl)-10,20-bis(2,4,6-trimethylphenyl)porphyrin (**7**), 7′-apo-7′-(4-acetamidophenyl)-*β*-carotene (**16**), and 7′-apo-7′-(4-aminophenyl)-*β*-carotene (**17**) were prepared by published procedures.[27,28]

*5-(4-Carboxyphenyl)-15-(4-carbomethoxyphenyl)-10,20-bis-(2,4,6-trimethylphenyl)porphyrin (**8**).* Porphyrin **7** (200 mg, 0.246 mmol) was dissolved in 40 mL of trifluoroacetic acid and 80 mL of concentrated hydrochloric acid and heated to 60 °C. When TLC indicated some formation of the diacid, the reaction was diluted with dichloromethane and neutralized with an aqueous solution of $NaHCO_3$. The organic layer was washed with water (× 3), dried over $Na_2SO_4$, and concentrated. Porphyrins **7** (145 mg) and **8** (50 mg, 26% yield) were isolated by column chromatography (silica gel, 1:9, methanol:dichloromethane). On the basis of recovered **7**, a yield of 90% was obtained. The recovered porphyrin (**7**) was recycled through the same process: $^1$H NMR (300 MHz, $CDCl_3$) $\delta$ −2.62 (2H, s, pyrrole −NH), 1.84 (12H, s, 10,20-Ar *o*-$CH_3$), 2.63 (6H, s, 10,20-Ar *p*-$CH_3$), 4.11 (3H, s, 15-Ar $-CO_2CH_3$), 7.28 (4H, s, 10,20-Ar −H), 8.32 (2H, d, $J$ = 8 Hz, 5-Ar −H), 8.38 (2H, d, $J$ = 8 Hz, 15-Ar −H), 8.44 (2H, d, $J$ = 8 Hz, 5-Ar −H), 8.57 (2H, d, $J$ = 8 Hz, 15-Ar −H) 8.71−8.79 (8H, m, pyrrole H-2, H-3, H-7, H-8, H-12, H-13, H-17, H-18); MALDI-TOF-MS *m*/*z* 800.3 ($C_{53}H_{44}N_4O_4^+$, calcd 800.3); UV−vis ($CH_2Cl_2$) 419, 515, 549, 590, 645 nm.

*5-(4-Carbomethoxyphenyl)-15-(N−tert-butoxy-4-aminophenyl)-10,20-bis(2,4,6-trimethylphenyl)porphyrin (**9**)* was prepared by dissolving 100 mg (0.125 mmol) of porphyrin **8** in 15 mL of *tert*-butyl alcohol and 25 $\mu$L (0.18 mmol) triethylamine. After the addition of 33 $\mu$L (0.16 mmol) of diphenylphosphoryl azide (DPPA) the solution was heated to 80 °C and stirred overnight. After 30 h, the reaction was diluted with dichloromethane, washed successively with diluted aqueous citric acid, saturated $NaHCO_3$(aq), and water, and then dried with $Na_2SO_4$ and concentrated. The product was isolated by column chromatography (silica gel, 1:19 ethyl acetate:toluene) in 69% yield (75 mg): $^1$H NMR (300 MHz, $CDCl_3$) $\delta$ −2.61 (2H, s, pyrrole −NH), 1.65 (9H, s, 15-Ar $-CO_2CH(CH_3)_3$), 1.85 (12H, s, 10,20-Ar *o*-$CH_3$), 2.64 (6H, s, 10,20-Ar *p*-$CH_3$), 4.11 (3H, s, 5-Ar $-CO_2CH_3$), 6.85(1H, s, 15-Ar −NH), 7.29 (4H, s, 10,20-Ar −H), 7.77 (2H, d, $J$ = 8 Hz, 15-Ar −H), 8.15 (2H, d, $J$ = 8 Hz, 15-Ar −H), 8.32 (2H, d, $J$ = 8 Hz, 5-Ar −H), 8.44 (2H, d, $J$ = 8 Hz, 5-Ar −H), 8.70−8.75 (6H, m, pyrrole H-2, H-3, H-7, H-8, H-12, H-18), 8.85 (2H, d, $J$ = 5 Hz, pyrrole H-13, H-17); MALDI-TOF-MS *m*/*z* 871.4 ($C_{57}H_{53}N_5O_4^+$, calcd 871.4); UV−vis ($CH_2Cl_2$) 420, 516, 552, 591, 641 nm.

*5-(4-Carbomethoxyphenyl)-15-(4-aminophenyl)-10,20-bis-(2,4,6-trimethylphenyl)porphyrin (**10**).* Porphyrin **9** (50 mg, 0.057 mmol) was dissolved in 10 mL of dichloromethane, and 10 mL of trifluoroacetic acid was added. The solution was stirred at room temperature. TLC indicated that no starting material was present after 1 h. The solution was diluted with dichloromethane and neutralized with $NaHCO_3$(aq). The organic layer was washed with water (×3), dried with $Na_2SO_4$, and concentrated. Pure porphyrin **10** was obtained (44 mg, 99% yield): $^1$H NMR (300 MHz, $CDCl_3$) $\delta$ −2.59 (2H, s, pyrrole −NH), 1.85 (12H, s, 10,20-Ar *o*-$CH_3$), 2.64 (6H, s, 10,20-Ar *p*-$CH_3$), 4.01 (2H, bs, 15-Ar −$NH_2$), 4.11 (3H, s, 5-Ar −$CO_2CH_3$), 7.06 (2H, d, $J$ = 8 Hz, 15-Ar −H), 7.29 (4H, s, 10,20-Ar −H), 8.00 (2H, d, $J$ = 8 Hz, 15-Ar −H), 8.32 (2H, d, $J$ = 8 Hz, 5-Ar −H), 8.43 (2H, d, $J$ = 8 Hz, 5-Ar −H), 8.69−8.74 (6H, m, pyrrole H-2, H-3, H-7, H-8, H-12, H-18), 8.90 (2H, d, $J$ = 5 Hz, pyrrole H-13, H-17); MALDI-TOF-MS 772.6 *m*/*z* ($C_{52}H_{45}N_5O_2^+$, calcd 771.9); UV−vis ($CH_2Cl_2$) 422, 517, 553, 594, 649 nm.

*5-(4-Carboxyphenyl)-15-(4-aminophenyl)-10,20-bis(2,4,6-trimethylphenyl)porphyrin (**11**).* In a 50 mL round-bottomed flask fitted with a condenser, 30 mg (0.039 mmol) of porphyrin **10** in 12 mL of trifluoroacetic acid and 24 mL of concentrated hydrochloric acid was heated to 60 °C for 4 days under inert atmosphere. After TLC (1:9 methanol:dichloromethane) indicated that no starting material remained, the solution was diluted with dichloromethane and neutralized with $NaHCO_3$(aq). The organic layer was washed with water (×3) and dried with $Na_2SO_4$. Distillation of the solvent at reduced pressure resulted in 49 mg (99% yield) of porphyrin **11**: $^1$H NMR (300 MHz, $CDCl_3$) $\delta$ −2.57 (2H, s, pyrrole −NH), 1.86 (12H, s, 10,20-Ar *o*-$CH_3$), 2.65 (6H, s, 10,20-Ar *p*-$CH_3$), 4.01 (2H, bs, 15-Ar−$NH_2$) 7.07 (2H, d, $J$ = 8 Hz, 15-Ar −H), 7.30 (4H, s, 10,20-Ar −H), 8.02 (2H, d, $J$ = 8 Hz, 15-Ar −H), 8.39 (2H, d, $J$ = 8 Hz, 5-Ar −H), 8.55 (2H, d, $J$ = 8 Hz, 5-Ar −H), 8.70−8.78 (6H, m, pyrrole H-2, H-3, H-7, H-8, H-12, H-18), 8.92 (2H, d, $J$ = 5 Hz, pyrrole H-13, H-17); MALDI-TOF-MS *m*/*z* 758 ($C_{51}H_{43}N_5O_2^+$, calcd 758); UV−vis ($CH_2Cl_2$) 421, 517, 554, 590, 647 nm.

*5-(4-Carbomethoxyphenyl)-15-(4-acetamidophenyl)-10,20-bis(2,4,6-trimethylphenyl)porphyrin (**3**).* Porphyrin **10** (14 mg, 0.018 mmol) was stirred at 80 °C in 14 mL of acetic anhydride and 0.5 mL of pyridine for 2 h. The reaction was quenched with water while the solution was still warm. The organic layer was washed with water (×3), dried with $Na_2SO_4$, and concentrated. Porphyrin **3** (13 mg, 88% yield) was obtained after purification by column chromatography (silica gel, 1:4 ethyl acetate:toluene): $^1$H NMR (300 MHz, $CDCl_3$) $\delta$ −2.63 (2H, s, pyrrole −NH), 1.84 (12H, s, 10,20-Ar *o*-$CH_3$), 2.36 (3H, s, 15-Ar −$COCH_3$), 2.63 (6H, s, 10,20-Ar *p*-$CH_3$), 4.11 (3H, s, 5-Ar −$CO_2CH_3$), 7.28 (4H, s, 10,20-Ar −H), 7.53 (1H, s, 15-Ar −NH), 7.89 (2H, d, $J$ = 8 Hz, 15-Ar −H), 8.18 (2H, d, $J$ = 8 Hz, 15-Ar −H), 8.31 (2H, d, $J$ = 8 Hz, 5-Ar −H), 8.43 (2H, d, $J$ = 8 Hz, 5-Ar −H), 8.69−8.75 (6H, m, pyrrole H-2, H-3, H-7, H-8, H-12, H-18), 8.82 (2H, d, $J$ = 5 Hz, pyrrole H-13, H-18); MALDI-TOF-MS *m*/*z* 814.1 ($C_{54}H_{47}N_5O_3^+$, calcd 814); UV−vis ($CH_2Cl_2$) 420, 516, 551, 590, 647 nm.

*5-(Heptafluoropropyl)dipyrromethane (**12**).* Pyrrole (3.5 mL, 50 mmol), heptafluorobutyraldehyde (5.0 g, 25 mmol), and 100 mL of freshly distilled tetrahydrofuran were degassed for 15 min by bubbling with $N_2$. Concentrated hydrochloric acid (2 mL) was added and the mixture was refluxed for 2 h under $N_2$. The solution was neutralized with $NaHCO_3$(aq) and then diluted with dichloromethane. The organic layer was washed with saturated $NaHCO_3$(aq) (×2) and water, dried with $Na_2SO_4$, and concentrated. Compound **12** (3.36 g, 42% yield) was isolated by column chromatography (silica gel, 1:1 hexanes:dichloromethane): $^1$H NMR (300 MHz, $CDCl_3$) $\delta$ 4.94 (1H, t, $J$ = 17 Hz, meso H-5), 6.18−6.24 (4H, m, pyrrole H-3, H-4), 6.77−6.79 (2H, m, pyrrole H-2), 6.12 (2H, bs, pyrrole −NH).

*5,10,15,20-Tetrakis(heptafluoropropyl)porphyrin (**13**), 5-(4-carbomethoxyphenyl)-10,15,20-tris(heptafluoropropyl)porphyrin (**4**), and 5,15-bis(4-carbomethoxyphenyl)-10,20-bis-(heptafluoropropyl)porphyrin (**14**).* In a 1000 mL round-bottomed flask, 1.9 g (6.0 mmol) of 5-(heptafluoropropyl)-dipyrromethane (**12**), and 500 mL of dichloromethane were degassed by bubbling with $N_2$ for 15 min. To this solution, 0.594 g (3.00 mmol) of heptafluorobutyraldehyde, 0.492 g (3.00 mmol) of methyl 4-formylbenzoate, and 0.03 mL (0.30 mmol) of boron trifluoride diethyl etherate were added. After the mixture turned a deep purple color (approximately 24 h), 0.681 g (3.00 mmol) of 2,3-dichloro-5,6-dicyanobenzoquinone (DDQ) was added and the stirring was continued for 24 h. The DDQ was removed by chromatography through a pad of silica until the eluent was tan-colored. The solvent was removed and the product dissolved in 500 mL of toluene. The treatment with DDQ was repeated with 0.681 g (3.00 mmol) and the solution was refluxed for 48 h. Again, the DDQ was removed by chromatography through a pad of silica. The residue was purified by column chromatography (silica, 1:1 hexanes:dichloromethane). Three major products were formed. *5,10,15,20-Tetrakis(heptafluoropropyl)porphyrin (**13**):* 100 mg (3% yield); $^1$H NMR (300 MHz, $CDCl_3$) $\delta$ −2.28 (2H, s, pyrrole −NH), 9.92 (8H, s, pyrrole H-2, H-3, H-7, H-8, H-12, H-13, H-17, H-18); MALDI-TOF-MS *m*/*z* 983.2 ($C_{32}H_{10}F_{28}N_4^+$ calcd 982.4); UV−vis ($CH_2Cl_2$) 409, 510, 541, 589, 649 nm. *5-(4-Carbomethoxyphenyl)-10,15,20-tris(heptafluoropropyl)porphyrin (**4**):* 167 mg (6% yield); $^1$H NMR (300 MHz, $CDCl_3$) $\delta$ −2.40 (2H, s, pyrrole −NH), 4.13 (3H, s, 5-Ar −$CO_2CH_3$), 8.46 (2H, d, $J$ = 8 Hz, 5-Ar −H), 8.81 (2H, d, $J$ = 8 Hz, 5-Ar −H), 9.38 (2H, bs, pyrrole H-3, H-7), 9.57 (6H, bs, pyrrole H-2, H-8, H-12, H-13, H-17, H-18); MALDI-TOF-MS *m*/*z* 947.4 ($C_{37}H_{17}F_{21}N_4O_2^+$, calcd 848); UV−vis ($CH_2Cl_2$) 410, 512, 545, 589, 643 nm. *5,15-Bis(4-carbomethoxyphenyl)-10,20-bis(heptafluoropropyl)porphyrin (**14**):* 558 mg (20% yield); $^1$H NMR (300 MHz, $CDCl_3$) $\delta$ −2.55 (2H, s, pyrrole −NH), 4.15 (6H, s, 5, 15-Ar −$CO_2CH_3$), 8.26 (4H, d, $J$ = 8 Hz, 5, 15-Ar −H), 8.47 (4H, d, $J$ = 8 Hz, 5, 15-Ar −H), 8.86 (4H, d, $J$ = 6 Hz, pyrrole H-3, H-7, H-13, H-17), 9.48 (4H, bs, pyrrole H-2, H-8, H-12, H-18); MALDI-TOF-MS *m*/*z* 915.2 ($C_{42}H_{24}F_{14}N_4O_4^+$, calcd 915); UV−vis ($CH_2Cl_2$) 411, 512, 547, 591, 644 nm.

*5-(4-Carboxyphenyl)-10,15,20-tris(heptafluoropropyl)porphyrin (**15**)* was prepared by dissolving 160 mg (0.170 mmol) of porphyrin **4** in 40 mL of trifluoroacetic acid and 80 mL of concentrated hydrochloric acid. The solution was stirred at 60 °C overnight. After that time, the reaction mixture was diluted with dichloromethane and neutralized with aqueous $NaHCO_3$. The organic layer was washed with water (× 3), dried with $Na_2SO_4$, and concentrated. Porphyrin **15** (114 mg, 72% yield) was isolated by column chromatography (silica gel, 1:9 methanol:dichloromethane). The starting material, porphyrin **4**, could also be recovered (30 mg): $^1$H NMR (300 MHz, $CDCl_3$) $\delta$ −2.38 (2H, s, pyrrole −NH), 8.57 (2H, d, $J$ = 8 Hz, 5-Ar −H), 8.84 (2H, d, $J$ = 8 Hz, 5-Ar −H), 9.40 (2H, bs, pyrrole H-3, H-7), 9.58 (6H, bs, pyrrole H-2, H-8, H-12, H-13, H-17, H-18); MALDI-TOF-MS *m*/*z* 934.8 ($C_{36}H_{15}F_{21}N_4O_2^+$, calcd 934.5); UV−vis ($CH_2Cl_2$) 410, 512, 545, 590, 642 nm.

*$P_F$-P−COOH, Dyad **18***. In a dry 100 mL round-bottomed flask under an argon atmosphere, 35 mg (0.037 mmol) of fluorinated porphyrin (**15**) was dissolved in 25 mL of dry toluene and 1 mL of pyridine. To this solution, 4 $\mu$L (0.05 mmol) of thionyl chloride was added, and the stirring was continued. The acid chloride formation was monitored by quenching a small aliquot in 1:9 methanol:dichloromethane and a TLC was run every 15 min. After the acid chloride formed, about 1 h, excess thionyl chloride and solvent was removed by evaporation at reduced pressure. The acid chloride in 5 mL of toluene and 0.5 mL of pyridine was added dropwise to a solution of 14 mg (0.018 mmol) of porphyrin **11** in 15 mL of toluene and 0.5 mL of pyridine. After 1 h the reaction was quenched with water and washed with water (×3). The organic layer was dried with $Na_2SO_4$ and concentrated. Column chromatography (silica gel, 1:9 methanol:dichloromethane) resulted in 15 mg (50% yield) of **18**: $^1$H NMR (300 MHz, $CDCl_3$) $\delta$ −2.57 (2H, s, $P_M$ pyrrole −NH), −2.34 (2H, s, $P_F$ pyrrole −NH), 1.87 (12H, s, $P_M$ 10,20-Ar *o*-$CH_3$), 2.66 (6H, s, $P_M$ 10,20-Ar *p*-$CH_3$), 7.31 (4H, s, $P_M$ 10,20-Ar −H), 8.22−8.57 (12H, m, $P_M$ 5, 15-Ar −H, $P_F$ 5-Ar −H), 8.74−8.80 (6H, m, $P_M$ pyrrole H-2, H-3, H-7, H-8, H-12, H-18), 8.91−8.94 (4H, m, $P_M$ pyrrole H-13, H-17, $P_F$ pyrrole H-2, H-7), 9.45 (2H, bs, $P_F$ pyrrole H-3, H-8), 9.60 (4H, bs, $P_F$ pyrrole H-12, H-13, H-17, H-18); MALDI-TOF-MS *m*/*z* 1673.8 ($C_{87}H_{56}F_{21}N_9O_3^+$, calcd 1674.4); UV−vis ($CH_2Cl_2$) 421, 515, 549, 591, 645 nm.

*C−P−$P_F$, Triad **1***. In a dry 100 mL round-bottomed flask under argon atmosphere, 15 mg (0.01 mmol) of dyad **18** was dissolved in 20 mL of dry toluene and 1 mL of pyridine. A portion of thionyl chloride (2 $\mu$L, 0.03 mmol) was added and the mixture was kept well-stirred. TLC was used to check the progress of the reaction, in the same fashion as for dyad **18**. Excess thionyl chloride and solvent were removed under vacuum. To a solution of the acid chloride in 15 mL of dry toluene and 0.5 mL pyridine was added 10 mg (0.02 mmol) of aminocarotenoid **17** in 5 mL of dry toluene and 0.5 mL of pyridine. After 1 h of stirring, the reaction mixture was quenched with water and then washed with water (× 3). The organic layer was dried with $Na_2SO_4$ and concentrated. Triad **1** (17 mg, 89% yield) was isolated by column chromatography (silica gel, 3:7 hexanes:dichloromethane): $^1$H NMR (500 MHz, $CDCl_3$) $\delta$ −2.56 (2H, s, $P_M$ pyrrole −NH), −2.34 (2H, s, $P_F$ pyrrole −NH), 1.04 (6H, s, car H-16, H-17), 1.44−1.49 (2H, m, car H-2), 1.58−1.64 (2H, m, car H-3), 1.72 (3H, s, car H-18), 1.88 (12H, s, $P_M$ 10,20-Ar *o*-$CH_3$), 1.98−2.01 (14H, m, car H-4, H-19, H-20, H-20′, H-19′), 2.65 (6H, s, $P_M$ 10,20-Ar *p*-$CH_3$), 6.12−6.86 (14H, m, car vinyl −CH), 7.32 (4H, s, $P_M$ 10,20-Ar −H), 7.55 (2H, d, $J$ = 8 Hz, car H-1′, H-5′), 7.79 (2H, d, $J$ = 8 Hz, car H-2′, H-4′), 8.14−8.49 (12H, m, $P_M$ 5, 15-Ar −H, $P_F$ 5-Ar −H), 8.74−8.79 (6H, m, $P_M$ pyrrole H-2, H-3, H-7, H-8, H-12, H-18), 8.91−8.94 (4H, m, $P_M$ pyrrole H-13, H-17, $P_F$ pyrrole H-3, H-7), 9.45 (2H, bs, $P_F$ pyrrole H-2, H-8), 9.60 (4H, bs, $P_F$ pyrrole H-12, H-13, H-17, H-18); MALDI-TOF-MS *m*/*z* 2162.7 ($C_{124}H_{101}F_{21}N_{10}O_2^+$, calcd 2162); UV−vis ($CH_2Cl_2$) 421, 477, 511, 591, 644 nm.

*$P_F$−P−$COOCH_3$, Dyad **2***. In a dry 100 mL round-bottomed flask under argon atmosphere, 34 mg (0.037 mmol) of fluorinated porphyrin (**15**) was dissolved in 25 mL of dry toluene and 1 mL of pyridine. To this solution, 10 $\mu$L (0.06 mmol) of thionyl chloride was added, and the stirring was continued for 1 h. After the acid chloride formed, excess thionyl chloride and solvent were removed by evaporation under reduced pressure. The acid chloride in 5 mL of toluene and 0.5 mL of pyridine was added dropwise to a solution of 14 mg (0.02 mmol) of porphyrin **10** in 15 mL of toluene and 0.5 mL of pyridine. After 1 h the reaction was quenched with water and washed with water (×3). The organic layer was dried with $Na_2SO_4$ and concentrated. Column chromatography (silica gel, dichloromethane) gave 15 mg (57% yield) of compound **2**. $^1$H NMR (500 MHz, $CDCl_3$) $\delta$ −2.57 (2H, s, $P_M$ pyrrole −NH), −2.34 (2H, s, $P_F$ pyrrole −NH), 1.87 (12H, s, $P_M$ 10,20-Ar *o*-$CH_3$), 2.65 (6H, s, $P_M$ 10,20-Ar *p*-$CH_3$), 4.11 (3H, s, $P_M$ 5-Ar −$CO_2CH_3$), 7.31 (4H, s, $P_M$ 10,20-Ar −H), 8.23 (2H, d, $J$ = 8 Hz, $P_M$ 15-Ar −H), 8.33 (2H, d, $J$ = 8 Hz, $P_M$ 5-Ar −H), 8.35 (2H, d, $J$ = 8 Hz, $P_M$ 15-Ar −H), 8.44 (2H, d, $J$ = 8 Hz, $P_M$ 5-Ar −H), 8.47−8.51 (4H, m, $P_F$ 5-Ar −H), 8.73−8.77 (6H, m, $P_M$ pyrrole H-2, H-3, H-7, H-8, H-12, H-18), 8.91−8.94 (4H, m, $P_M$ pyrrole H-13, H-17, $P_F$ pyrrole H-3, H-7), 9.45 (2H, bs, $P_F$ pyrrole H-2, H-8), 9.60 (4H, bs, $P_F$ pyrrole H-12, H-13, H-17, H-18); MALDI-TOF-MS *m*/*z* 1687.4 ($C_{88}H_{58}F_{21}N_9O_3^+$, calcd 1687.4); UV−vis ($CH_2Cl_2$) 420, 514, 548, 590, 644 nm.

*5-(4-Carboxyphenyl)-15-(4-trifluoroacetamidophenyl)-10,20-bis(2,4,6-trimethylphenyl)porphyrin (**19**)*. At 0 °C 1 mL of trifluoroacetic anhydride was added to a solution of 50 mg (0.066 mmol) of porphyrin **11** in 25 mL of dichloromethane. The dark green solution was quenched after 1 h by pouring the solution into 50 mL of dichloromethane and washing with water (× 6). The organic layer was dried over $Na_2SO_4$ and concentrated under reduced pressure. Porphyrin **19** was purified by column chromatography (silica gel, 1:9 methanol:dichloromethane) to yield 54 mg (96% yield): $^1$H NMR (300 MHz, $CDCl_3$) $\delta$ −2.63 (2H, s, pyrrole −H), 1.83 (12H, s, 10,20-Ar *o*-$CH_3$), 2.62 (6H, s, 10,20-Ar *p*-$CH_3$), 7.28 (4H, s, 10,20-Ar −H), 7.98 (2H, d, $J$ = 9 Hz, 15-Ar −H), 8.21 (1H, s, 15-Ar −NH) 8.27 (2H, d, $J$ = 9 Hz, 15-Ar −H), 8.78 (2H, d, $J$ = 9 Hz, 5-Ar −H), 8.56 (2H, d, $J$ = 9 Hz, 5-Ar −H), 8.71−8.78 (8H, m, pyrrole H-2, H-3, H-7, H-8, H-12, H-13, H-17, H-18); MALDI-TOF-MS *m*/*z* 853.3 ($C_{53}H_{42}F_3N_5O_3^+$, calcd 853.3); UV−vis ($CH_2Cl_2$) 420, 516, 551, 592, 648 nm.

*C−P−$NHCOCF_3$, Dyad **20***, was prepared by dissolving 35 mg (0.041 mmol) of porphyrin **19** in 10 mL of dry toluene and 0.2 mL of pyridine under argon atmosphere. A portion of 10 $\mu$L (0.12 mmol) of thionyl chloride was added and the stirring continued for 1 h. After the acid chloride was formed, the excess thionyl chloride and solvent were removed. The acid chloride was dissolved in 10 mL of dry dichloromethane and 0.2 mL of pyridine. Finally, 41 mg (0.082 mmol) of carotenoid **17** was added and the stirring was continued for 1 h. After 1 h, the reaction was quenched with water. The organic layer was washed with water (×3), dried over $Na_2SO_4$, and concentrated under reduced pressure. After column chromatography (silica gel, 1:0.1:9 ethyl acetate:triethylamine:toluene), 17 mg (32% yield) of dyad **20** was obtained: $^1$H NMR (300 MHz, $CDCl_3$) $\delta$ 2.63 (2H, s, pyrrole −NH), 1.04 (6H, s, car H-16, H-17), 1.47−1.49 (2H, m, car H-2), 1.60−1.62 (2H, m, car H-3), 1.73 (3H, s, car H-18), 1.85 (12H, s, $P_M$ 10,20-Ar *o*-$CH_3$), 1.98−2.01 (14H, m, car H-4, H-19, H-20, H-19′, H-20), 2.63 (6H, s, $P_M$ 10,20-Ar *p*-$CH_3$), 6.12−6.96 (14H, m, car vinyl −CH), 7.29 (4H, s, $P_M$ 10,20-Ar −H), 7.54 (2H, d, $J$ = 8 Hz, car H-1′, H-5′), 7.78 (2H, d, $J$ = 8 Hz, car H-2′, H-4′), 7.99 (2H, d, $J$ = 8 Hz, $P_M$ 15-Ar −H), 8.17 (1H, s, $P_M$ 15-Ar −NH), 8.25−8.28 (4H, m, $P_M$ 5-Ar −H, 15-Ar −H), 8.37 (2H, d, $J$ = 8 Hz, $P_M$ 5-Ar −H), 8.72−8.79 (8H, m, $P_M$ pyrrole H-2, H-3, H-7, H-8, H-12, H-13, H-17, H-18); MALDI-TOF-MS *m*/*z* 1340.7 ($C_{90}H_{87}F_3N_6O_2^+$, calcd 1340.7); UV−vis ($CH_2Cl_2$) 300, 374, 422, 480, 512, 592, 650 nm.

*C−P−$NH_2$, Dyad **21***. Dyad **20** (17 mg, 0.013 mmol) was deprotected by stirring in 6 mL of tetrahydrofuran and 20 mL

of freshly prepared methanolic potassium hydroxide for 36 h at 40 °C. The reaction was quenched by pouring the solution into ethyl ether and then washing the organic phase with water (×6). The organic solution was dried with $Na_2SO_4$ and concentrated under reduced pressure. Purification by column chromatography (silica gel, 1:0.1:99 ethyl acetate:triethylamine: toluene) resulted in 14 mg (91% yield) of dyad **21**: $^1$H NMR (300 MHz, $CDCl_3$) $\delta$ −2.63 (2H, s, pyrrole −NH), 1.04 (6H, s, car H-16, H-17), 1.44−1.49 (2H, m, car H-2), 1.61−1.66 (2H, m, car H-3), 1.73 (3H, s, car H-18), 1.85 (12H, s, $P_M$ 10,20-Ar *o*-$CH_3$), 1.98−2.08 (14H, m, car H-4, H-19, H-20, H-19′, H-20), 2.63 (6H, s, $P_M$ 10,20-Ar *p*-$CH_3$), 4.03 (2H, s, $P_M$ 15-Ar −$NH_2$), 6.15−6.96 (14H, m, car vinyl −CH), 7.06 (2H, d, $J$ = 8 Hz, $P_M$ 15-Ar −H), 7.29 (4H, s, $P_M$ 10,20-Ar −H), 7.54 (2H, d, $J$ = 8 Hz, car H-1′, H-5′), 7.78 (2H, d, $J$ = 8 Hz, car H-2′, H-4′), 8.00 (2H, d, $J$ = 8 Hz, $P_M$ 15-Ar −H), 8.25 (2H, d, $J$ = 8 Hz, $P_M$ 5-Ar −H), 8.36 (2H, d, $J$ = 8 Hz, $P_M$ 5-Ar −H), 8.68−8.75 (6H, m, $P_M$ pyrrole H-2, H-3, H-7, H-8, H-12, H-18) 8.89−8.91 (2H, m $P_M$ pyrrole H-13, H-18); MALDI-TOF-MS *m*/*z* 1244.7 ($C_{88}H_{88}N_6O^+$, calcd 1244.7); UV−vis ($CH_2Cl_2$) 300, 373, 422, 509, 550, 594, 649 nm.

*C−P−NHCOCH$_3$, Dyad **5***. Acetic anhydride (1 $\mu$L, 0.01 mmol) was added to a solution of 7 mg (0.006 mmol) of dyad **21** in 5 mL of dichloromethane and 2 $\mu$L of pyridine. After 2 h of stirring, the solution was diluted with dichloromethane and washed with water (×5). The organic layer was dried over $Na_2SO_4$ and concentrated. After column chromatography (silica gel, 1:4 ethyl acetate:toluene), 5 mg (70% yield) of dyad **5** was obtained: $^1$H NMR (300 MHz, $CDCl_3$) $\delta$ −2.62 (2H, s, pyrrole −NH), 1.04 (6H, s, car H-16, H-17), 1.42−1.49 (2H, m, car H-2), 1.61−1.64 (2H, m, car H-3), 1.73 (3H, s, car H-18), 1.85 (12H, s, $P_M$ 10,20-Ar *o*-$CH_3$), 1.98−2.08 (14H, m, car H-4, H-19, H-20, H-19′, H-20), 2.36 (3H, s, $P_M$ 15-Ar −$COCH_3$), 2.63 (6H, s, $P_M$ 10,20-Ar *p*-$CH_3$), 6.14−6.96 (14H, m, car vinyl −CH), 7.30 (4H, s, $P_M$ 10,20-Ar −H), 7.51−7.55 (3H, m, car H-1′, H-5′, $P_M$ 15-Ar −NH), 7.78 (2H, d, $J$ = 8 Hz, car H-2′, H-4′), 7.90 (2H, d, $J$ = 8 Hz, $P_M$ 15-Ar −H), 8.17 (2H, d, $J$ = 8 Hz, $P_M$ 15-Ar −H), 8.26 (2H, d, $J$ = 9 Hz, $P_M$ 5-Ar −H), 8.37 (2H, d, $J$ = 9 Hz, $P_M$ 5-Ar −H), 8.70−8.83(8H, m, $P_M$ pyrrole H-2, H-3, H-7, H-8, H-12, H-13, H-17, H-18); MALDI-TOF-MS *m*/*z* 1286.7 ($C_{90}H_{90}N_6O_2^+$, calcd 1286.7); UV−vis ($CH_2Cl_2$) 300, 370, 417, 477, 510, 590, 648 nm.

*C−P$_{Zn}$−P$_F$, Triad **1′***. A portion of 2 mg (0.001 mmol) of triad **1** was dissolved in 0.5 mL of dichloromethane. To this solution 0.5 mL of 0.001 M zinc acetate dissolved in 10% methanol/dichloromethane was added and the stirring was continued at room temperature for 12 h. After 12 h, an additional 0.5 mL aliquot of the zinc acetate solution was added and the stirring was continued for 6 h until a third compound was apparent by TLC (the dimetalated triad). The reaction mixture was immediately purified by column chromatography (silica gel, dichloromethane) to yield 0.5 mg of **1′** (25% yield): $^1$H NMR (500 MHz, $CDCl_3$) $\delta$ −2.34 (2H, s, $P_F$ pyrrole, −NH), 1.04 (6H, s, car H-16, H-17), 1.44−1.49 (2H, m, car H-2), 1.59−1.64 (2H, m, H-3), 1.87 (12H, s, $P_M$ 10,20-Ar *o*-$CH_3$) 1.98−2.09 (14H, m, car H-4, H-19, H-20, H-19′, H-20′), 2.66 (6H, s, $P_M$ 10,20-Ar *p*-$CH_3$), 6.12−6.95 (14H, m, car vinyl −CH), 7.32 (4H, s, $P_M$ 10, 20 Ar −H), 7.54 (2H, d, $J$ = 9 Hz, car H-1′, H-5′), 7.79 (2H, d, $J$ = 9 Hz, car H-2′, H-4′), 8.14−8.49 (12H, m, $P_M$ 5, 15-Ar −H, $P_F$ 5-Ar −H), 8.83−8.87 (6H, m, $P_M$ pyrrole H-2, H-3, H-7, H-8, H-12, H-18), 8.92 (2H, d, $J$ = 6 Hz, $P_M$ pyrrole H-13, H-17), 9.02 (2H, d, $J$ = 5 Hz, $P_F$ pyrrole H-3, H-7), 9.45 (2H, bs, $P_F$ pyrrole H-2, H-8), 9.60 (4H, bs, $P_F$ H-12, H-13, H-17, H-18); MALDI-TOF-MS *m*/*z* 2222.7 ($C_{124}H_{99}F_{21}N_{10}O_2Zn^+$, calcd 2222.7); UV−vis ($CH_2Cl_2$) 422, 478, 512, 545, 587, 641 nm.

*P$_F$−P$_{Zn}$−COOCH$_3$, Dyad **2′***. A portion of 2 mg (0.001 mmol) of dyad **2** was dissolved in 0.5 mL of dichloromethane. To this solution was added 0.5 mL of 0.0025 M zinc acetate dissolved in 10% methanol/dichloromethane, and the stirring continued at room temperature for 12 h. After 12 h, an additional 0.5 mL aliquot of the zinc acetate solution was added and the stirring was continued for another 6 h until a third compound was apparent by TLC (the dimetalated triad). The reaction mixture was immediately purified by column chromatography (silica gel, dichloromethane) to yield 0.5 mg (24% yield): $^1$H NMR (500 MHz, $CDCl_3$) $\delta$ −2.34 (2H, s, $P_F$ pyrrole −NH), 1.87 (12H, s, $P_M$ 10,20-Ar *o*-$CH_3$), 2.66 (6H, s, $P_M$ 10,20-Ar *p*-$CH_3$), 4.12 (3H, s, $P_M$ 5-Ar −$CO_2CH_3$), 7.23 (4H, s, $P_M$ 10,20-Ar −H), 8.22 (2H, d, $J$ = 8 Hz, $P_M$ 15-Ar −H), 8.35 (2H, d, $J$ = 8 Hz, $P_M$ 5-Ar −H), 8.37 (2H, d, $J$ = 8 Hz, $P_M$ 15-Ar −H), 8.45 (2H, d, $J$ = 8 Hz, $P_M$ 5-Ar −H), 8.47−8.51 (4H, m, $P_F$ 5-Ar −H), 8,82−8.86 (6H, m, $P_M$ pyrrole H-2, H-3, H-7, H-8, H-12, H-18), 8.93 (2H, d, $J$ = 5 Hz, $P_M$ pyrrole H-13, H-17), 9.02 (2H, d, $J$ = 5 Hz, $P_F$ pyrrole H-3, H-7), 9.46 (2H, bs, $P_F$ pyrrole H-2, H-8), 9.60 (4H, bs, $P_F$ pyrrole H-12, H-13, H-17, H-18); MALDI-TOF-MS *m*/*z* 1749.4 ($C_{88}H_{56}F_{21}N_9O_3Zn^+$, calcd 1749.3); UV−vis ($CH_2Cl_2$) 422, 510, 549, 587, 642 nm.

*Zinc 5-(4-Carbomethoxyphenyl)-15-(4-acetamidophenyl)-10,20-bis(2,4,6-trimethylphenyl)porphyrin (**3′**)*. A portion of 7 mg (0.009 mmol) of porphyrin **3** was stirred overnight in 1 mL of dichloromethane and an excess of 0.01 M zinc acetate dissolved in 10% methanol/dichloromethane. The reaction was worked up by diluting the solution with dichloromethane and washing (×3) with $H_2O$. The organic layer was dried with $Na_2SO_4$ and concentrated. The resulting **3′** was obtained in quantitative yield (8 mg): $^1$H NMR (500 MHz, $CDCl_3$) $\delta$ 1.82 (12H, s, 10,20-Ar *o*-$CH_3$), 2.36 (3H, s, 15-Ar −$COCH_3$), 2.63 (6H, s, 10,20-Ar *p*-$CH_3$), 4.11 (3H, s, 5-Ar −$CO_2CH_3$), 7.28 (4H, s, 10,20-Ar −H), 7.47 (1H, s, 15-Ar −NH), 7.86 (2H, d, $J$ = 8 Hz, 15-Ar −H), 8.16 (2H, d, $J$ = 8 Hz, 15-Ar −H), 8.30 (2H, d, $J$ = 8 Hz, 5-Ar −H), 8.39 (2H, d, $J$ = 8 Hz, 5-Ar −H), 8.71−8.76 (6H, m, pyrrole H-2, H-3, H-7, H-8, H-12, H-18), 8.83 (2H, d, $J$ = 5 Hz, pyrrole H-13, H-17); MALDI-TOF-MS *m*/*z* 875.3 ($C_{54}H_{45}N_5O_3Zn^+$, calcd 875.3); UV−vis ($CH_2Cl_2$) 419, 550, 591 nm.

*C−P$_{Zn}$−NHCOCH$_3$, Dyad **5′***. A portion of 2 mg (0.002 mmol) of dyad **5** was stirred overnight in 1 mL of dichloromethane with an excess of a solution of 0.01 M zinc acetate in 10% methanol/dichloromethane. The reaction was worked up by diluting the solution with dichloromethane and washing (×3) with $H_2O$. The organic layer was dried with $Na_2SO_4$ and concentrated. The resulting product was obtained in 95% yield (2 mg): $^1$H NMR (500 MHz, $CDCl_3$) $\delta$ 1.04 (6H, s, car H-17, H-16), 1.42−1.49 (2H, m, car H-2), 1.61−1.64 (2H, m, car H-3), 1.73 (3H, s, car H-18), 1.84 (12H, s, $P_M$ 10, 20 *o*-$CH_3$), 1.99−2.09 (14H, m, car H-4, H-19, H-20, H-19′, H-20′), 2.33 (3H, s, $P_M$ 15-Ar −$COCH_3$), 2.64 (6H, s, $P_M$ 10,20-Ar *p*-$CH_3$), 6.16−6.95 (14H, m, car vinyl −CH), 7.29 (4H, s, $P_M$ 10,20-Ar −H), 7.47 (1H, s, $P_M$ 15-Ar −NH), 7.54 (2H, d, $J$ = 9 Hz, car H-1′, H-5′), 7.77 (2H, d, $J$ = 9 Hz, car H-2′, H-4′), 7.86 (2H, d, $J$ = 8 Hz, $P_M$ 15-Ar −H), 8.18 (2H, d, $J$ = 8 Hz, $P_M$ 15-Ar −H), 8.24 (2H, d, $J$ = 8 Hz, $P_M$ 5-Ar −H), 8.38 (2H, d, $J$ = 8 Hz, $P_M$ 5-Ar −H), 8.77−8.90 (8H, m, $P_M$ pyrrole H-2, H-3, H-7, H-8, H-12, H-13, H-17, H-18); MALDI-TOF-MS *m*/*z* 1348.7 ($C_{90}H_{88}N_6O_2Zn^+$, calcd1348.6); UV−vis ($CH_2Cl_2$) 422, 477, 505, 546, 588 nm.

**Acknowledgment.** This work was supported by a grant from by the U.S. Department of Energy (DE-FG02-03ER15393). We thank Roche for the generous gift of carotenoid samples. This is publication 590 from the ASU Center for the Study of Early Events in Photosynthesis.

## References and Notes

(1) Gust, D.; Moore, T. A.; Moore, A. L. *Acc. Chem. Res.* **1993**, *26*, 198−205.
(2) Wasielewski, M. R. *Chem. Rev.* **1992**, *92*, 435−461.
(3) Gust, D.; Moore, T. A. In *The Porphyrin Handbook*; Kadish, K. M., Smith, K. M., Guilard, R., Eds.; Academic Press: New York, 1999; pp 153−190.
(4) Guldi, D. M. *Pure Appl. Chem.* **2003**, *75*, 1069−1075.
(5) Imahori, H.; Tamaki, K.; Guldi, D. M.; Luo, C. P.; Fujitsuka, M.; Ito, O.; Sakata, Y.; Fukuzumi, S. *J. Am. Chem. Soc.* **2001**, *123*, 2607−2617.
(6) Liddell, P. A.; Kuciauskas, D.; Sumida, J. P.; Nash, B.; Nguyen, D.; Moore, A. L.; Moore, T. A.; Gust, D. *J. Am. Chem. Soc.* **1997**, *119*, 1400−1405.
(7) Kuciauskas, D.; Liddell, P. A.; Lin, S.; Johnson, T. E.; Weghorn, S. J.; Lindsey, J. S.; Moore, A. L.; Moore, T. A.; Gust, D. *J. Am. Chem. Soc.* **1999**, *121*, 8604−8614.
(8) Guldi, D. M. *Chem. Soc. Rev.* **2002**, *31*, 22−36.
(9) Ohkubo, K.; Imahori, H.; Shao, J. G.; Ou, Z. P.; Kadish, K. M.; Chen, Y. H.; Zheng, G.; Pandey, R. K.; Fujitsuka, M.; Ito, O.; Fukuzumi, S. *J. Phys. Chem. A* **2002**, *106*, 10991−10998.
(10) Imahori, H.; Yamada, H.; Guldi, D. M.; Endo, Y.; Shimomura, A.; Kundu, S.; Yamada, K.; Okada, T.; Sakata, Y.; Fukuzumi, S. *Angew. Chem., Int. Ed. Engl.* **2002**, *41*, 2344−2347.
(11) Kuciauskas, D.; Liddell, P. A.; Lin, S.; Stone, S. G.; Moore, A. L.; Moore, T. A.; Gust, D. *J. Phys. Chem. B* **2000**, *104*, 4307−4321.
(12) Fukuzumi, S.; Nakanishi, I.; Suenobu, T.; Kadish, K. M. *J. Am. Chem. Soc.* **1999**, *121*, 3468−3474.
(13) Hush, N. S. *Trans. Faraday Soc.* **1961**, *57*, 557−580.
(14) Marcus, R. A. *J. Chem. Phys.* **1956**, *24*, 966−978.
(15) Hush, N. S. *J. Chem. Phys.* **1958**, *28*, 962−972.
(16) Marcus, R. A. *Can. J. Chem.* **1959**, *37*, 155−163.
(17) Kuciauskas, D.; Liddell, P.; Moore, T. A.; Moore, A. L.; Gust, D. In *Recent Advances in the Chemistry and Physics of Fullerenes and Related Materials*; Kadish, K. M., Ruoff, R. S., Eds.; The Electrochemical Society: Pennington, NJ, 1998; pp 242−261.
(18) Carbonera, D.; Di Valentin, M.; Corvaja, C.; Agostini, G.; Giacometti, G.; Liddell, P. A.; Kuciauskas, D.; Moore, A. L.; Moore, T. A.; Gust, D. *J. Am. Chem. Soc.* **1998**, *120*, 4398−4405.
(19) SteinbergYfrach, G.; Liddell, P. A.; Hung, S. C.; Moore, A. L.; Gust, D.; Moore, T. A. *Nature* **1997**, *385*, 239−241.
(20) Steinberg-Yfrach, G.; Rigaud, J. L.; Durantini, E. N.; Moore, A. L.; Gust, D.; Moore, T. A. *Nature* **1998**, *392*, 479−482.
(21) Bennett, I. M.; Vanegas Farfano, H. M.; Bogani, F.; Primak, A.; Liddell, P. A.; Otero, L.; Sereno, L.; Silber, J. J.; Moore, A. L.; Moore, T. A.; Gust, D. *Nature* **2002**, *420*, 401−403.
(22) Janot, J. M.; Bienvenue, E.; Seta, P.; Bensasson, R. V.; Tome, A. C.; Enes, R. F.; Cavaleiro, J. A. S.; Leach, S.; Camps, X.; Hirsch, A. *J. Chem. Soc. Perkin Trans. 2* **2000**, 301−306.
(23) Tronel-Peyroz, E.; Miquel-Mercier, G.; Vanel, P.; Seta, P. *Chem. Phys. Lett.* **1998**, *285*, 294−298.
(24) DeGraziano, J. M.; Macpherson, A. N.; Liddell, P. A.; Noss, L.; Sumida, J. P.; Seely, G. R.; Lewis, J. E.; Moore, A. L.; Moore, T. A.; Gust, D. *New J. Chem.* **1996**, *20*, 839−851.
(25) DeGraziano, J. M.; Liddell, P. A.; Leggett, L.; Moore, A. L.; Moore, T. A.; Gust, D. *J. Phys. Chem.* **1994**, *98*, 1758−1761.
(26) Kuciauskas, D.; Liddell, P. A.; Moore, A. L.; Moore, T. A.; Gust, D. *J. Am. Chem. Soc.* **1998**, *120*, 10880−10886.
(27) Lee, C. H.; Lindsey, J. S. *Tetrahedron* **1994**, *50*, 11427−11440.
(28) Gust, D.; Moore, T. A.; Moore, A. L.; Liddell, P. A. *Methods Enzymol.* **1992**, *213*, 87−100.
(29) Wijesekera, T. P. *Can. J. Chem.* **1996**, *74*, 1868−1871.
(30) Fungo, F.; Otero, L.; Durantini, E. N.; Silber, J. J.; Sereno, L.; Marino-Ochoa, E.; Moore, T. A.; Moore, A. L.; Gust, D. *J. Phys. Chem. B* **2001**, *105*, 4783−4790.
(31) Golub, G. H.; Reinsch, C. *Numer. Math.* **1970**, *14*, 403−420.
(32) Henry, E. R.; Hofrichter, J. *Methods Enzymol.* **1992**, *210*, 129−192.
(33) The time range used in this experiment (4.5 ns) is too short to accurately determine this time constant.
(34) Luo, C.; Guldi, D. M.; Imahori, H.; Tamaki, K.; Sakata, K. *J. Am. Chem. Soc.* **2000**, *122*, 6535−6551.
(35) Mosseri, S.; Mialocq, J. C.; Perly, B. *Radiat. Phys. Chem.* **1992**, *39*, 223−233.
(36) Hermant, R. M.; Liddell, P. A.; Lin, S.; Alden, R. G.; Kang, H. K.; Moore, A. L.; Moore, T. A.; Gust, D. *J. Am. Chem. Soc.* **1993**, *115*, 2080−2081.
(37) Bensasson, R. V.; Land, E. J.; Truscott, T. G. *Flash Photolysis and Pulse Radiolysis. Contribution to the Chemistry of Biology and Medicine*; Pergamon Press: New York, 1983.
(38) Bonnett, R.; McGarvey, D. J.; Harriman, A.; Land, E. J.; Truscott, T. G.; Winfield, U.-J. *Photochem. Photobiol.* **1988**, *48*, 271−276.
(39) Lewis, J. E.; Moore, T. A.; Benin, D.; Gust, D.; Nicodem, D.; Nonell, S. *Photochem. Photobiol.* **1994**, *59*, 35S.
(40) Demas, J. N. *Excited-state lifetimes*; Academic Press: New York, 1983.
(41) Kodis, G.; Liddell, P. A.; Moore, A. L.; Moore, T. A.; Gust, D. *J. Phys. Org. Chem.* **2004**, in press.
(42) Gust, D.; Moore, T. A.; Moore, A. L.; Krasnovsky, A. A.; Liddell, P. A.; Nicodem, D.; Degraziano, J. M.; Kerrigan, P.; Makings, L. R.; Pessiki, P. J. *J. Am. Chem. Soc.* **1993**, *115*, 5684−5691.
(43) Gust, D.; Moore, T. A.; Makings, L. R.; Liddell, P. A.; Nemeth, G. A.; Moore, A. L. *J. Am. Chem. Soc.* **1986**, *108*, 8028−8031.
(44) Osuka, A.; Yamada, H.; Shinoda, S.; Nozaki, K.; Ohno, T. *Chem. Phys. Lett.* **1995**, *238*, 37−41.
(45) Imahori, H.; Tamaki, K.; Araki, Y.; Sekiguchi, Y.; Ito, O.; Sakata, Y.; Fukuzumi, S. *J. Am. Chem. Soc.* **2002**, *124*, 5165−5174.
(46) Furutsuka, T.; Imura, T.; Kojima, T.; Kawabe, K. *Technol. Rep. Osaka University* **1974**, *24*, 367−369.
(47) Gaines, G. L.; O'Neil, M. P.; Svec, W. A.; Niemczyk, M. P.; Wasielewski, M. R. *J. Am. Chem. Soc.* **1991**, *113*, 719−721.
(48) Wasielewski, M. R.; Gaines, G. L.; O'Neil, M. P.; Svec, W. A.; Niemczyk, M. P.; Prodi, L.; Gosztola, D. J. In *Dynamics and Mechanisms of Photoinduced Transfer and Related Phenomena*; Mataga, N., Okada, T., Masuhara, H., Eds.; Elsevier Science Publishers: New York, 1992; pp 87−103.
(49) Davis, F. S.; Nemeth, G. A.; Anjo, D. M.; Makings, L. R.; Gust, D.; Moore, T. A. *Rev. Sci. Instrum.* **1987**, *58*, 1629−1631.
(50) Freiberg, A.; Timpmann, K.; Lin, S.; Woodbury, N. W. *J. Phys. Chem. B* **1998**, *102*, 10974−10982.